Lithologic Mapping of Mafic Intrusions in East Greenland Using Landsat Thematic Mapper Data.

H. R. Naslund

Department of Geological Sciences, State University of New York, Binghamton, NY 13901

R. W. Birnie

Department of Earth Sciences, Dartmouth College, Hanover, NH, 03755

J. T. Parr

The Analytical Sciences Corporation, Reading, MA, 01867

Final Report for Contract # NAS 5-28738

April 24, 1989

Table of Contents

Introduction

The East Greenland Tertiary Igneous Province contains a variety of intrusive and extrusive rock types. Intrusive rock units include layered tholeiitic gabbro sills, macro-dikes, and plutons; alkaline gabbro, syenite, and granite plutons; and several episodes of tholeiitic and alkaline dike swarms. Extrusive rock units include alkaline and tholeiitic flows, tuffs, and agglomerates, which form an 8 km thick sequence of flat lying plateau lavas. The majority of the igneous activity occurred during the period from 60 to 50 m.y. ago as Greenland was rifted from northern Europe during the opening of the north Atlantic Ocean. The intrusive rocks in the province form a series of plutonic centers exposed along an 800 km long segment of the East Greenland coast. The plateau lavas are exposed in the northern half of the province, but have been removed by erosion in the southern half. As a result, the host rocks for the plutonic centers in the northern half of the province are largely basaltic lavas, and the host rocks for the plutonic centers in the southern half of the province are largely Archean quartz-feldspar gneisses and amphibolites. Additional volcanic rocks and plutonic centers may be present in the province offshore or under the inland ice field. Layered tholeiitic intrusions are the primary sources of Pt and Pd, two strategic metals for which South Africa and the Soviet Union are the principal producers and the United States and Japan are the largest consumers. This study was initiated with the idea of using TM data to help locate potential Pt and Pd targets in the layered tholeiitic intrusions of the East Greenland Tertiary Igneous Province.

The Skaergaard complex is the most well known of the intrusive centers. It contains a central layered tholeiitic pluton, several associated

layered tholeiitic macro-dykes and sills, and numerous quartz and felspar-rich granophyric bodies ranging from dikes only cms wide to sills up to 100 m thick. The central pluton, which is approximately 5 by 8 kms in plan view, has undergone an extensive differentiation history from an initial Mg-rich magma to a final Fe-rich magma. This differentiation history is recorded in the rocks which crystallized on the floor (the Layered Series), the walls (the Marginal Border Series), and the roof (the Upper Border Series) of the magma chamber. A number of distinctive rock types were formed during this differentiation process, and include from the base of the intrusion upward (i.e. within the Layered Series): olivine-pyroxene-plagioclase gabbro (Lower Zone 1); olivine-pyroxene-plagioclase-magnetite gabbro (Lower Zone 2); pyroxene-plagioclase-magnetite gabbro (Middle Zone); fayalite-pyroxene- plagioclase-magnetite gabbro (Upper Zone 1); and fayalite-pyroxene- plagioclase-magnetite-apatite gabbro (Upper Zone 2). In addition to mineralogical units within the pluton, additional units can be defined on the basis of grain-size and texture. In particular the units of the Upper Border Series are coarser grained than those of the Layered Series, and the units of the Marginal Border Series are texturally distinct from those of the Layered or Upper border Series. The systematic variation in the chemical composition of the magma as it crystallized, resulted in recognizable gradational variations within many of the units (particularly with regard to iron content). TM data has been used to try to identify two types of changes in the intrusion: (1) abrupt changes in rock type caused by the presence or absence of particular mineral phases, and (2) gradational changes in rock type caused by systematic compositional variations. The host rocks for the

Skaergard intrusion, which is located in the middle of the province, include Archean gneiss and amphibolite on one side and Tertiary basaltic lavas on the other. The Skaergaard complex was chosen as the training site for this project because of the excellent exposures, the variety of rock types present, and because the geology of the complex is well known. It was hoped that information gained from TM analysis of the Skaergaard intrusion could be applied to other intrusive complexes in the province where the access is more difficult and the geology is not as well understood.

Field Research

A 1985 expedition to the field area consisted of five scientists: Dr. H. R. Naslund, P. A. Turner, D. W. Keith, J. Urquhart, and C. B. Brinkema. Our field research was concentrated on the area in the vicinity of the Skaergaard intrusion. During the field season a number of representative areas were chosen for each of the rock types that we hoped to map with the TM data. We also noted areas with unusual surface conditions (gravel cover, scattered snow patches, mineral staining, etc.). Owing to technical problems with the satellite, we were only able to receive TM data from two 1985 scenes: one collected on July 24th; and one collected on August 9th. Because of the heavier snow and poorer weather conditions for the July 24th scene, we have concentrated our data interpretation efforts on the August 9th scene. In addition to identifying test sites for Landsat mapping we collected a number of rock samples in order to determine representative rock compositions and to evaluate Pt/Pd resourse potential. These samples were used to complete three masters thesis projects, and one bachelors degree project.

Ten scientists accompanied the 1986 expedition to East Greenland, August 2nd 1986 to September 2nd 1986. Expedition members included Dr. H. R. Naslund, Dr. R. W. Birnie, Dr. Robert Bindschadler, Daniel Barnett, Jennifer Nichols, Max Cobb, J. T. Parr, P. A. Turner, James Foster, and Mark Hirschman. During the 1986 field season we examined areas where our earlier TM data were not able to distinguish different rock types, in order to determine what surface features interfere with the TM mapping technique. We also examined areas where we obtained different TM signatures from what we had assumed were identical rock types. Field work was directed toward collecting TM spectra of representative rock and snow units using a tripod-mounted ratioing spectrometer (HHRR). The HHRR allows direct correlation of observations made in the field to the TM data collected by the satellite, and can be used to determine what surface features most strongly affect the TM signature recorded for the 30 x 30 meter pixels. The HHRR receives a signal from an approximately 100 cm^2 area, so it can be used to compare the TM signatures for a variety of surface conditions (wet rock, dry rock, weathered rock, unweathered rock, stained rock, fresh rock, etc.). Test spectra of plant materials, mineral stains, and soil areas were also collected. Additional rock samples were collected from the Skaergaard intrusion and from the Kraemer Island Macrodyke intrusion. Field Results were used to complete one masters thesis and two bachelors theses.

During the 1986 field season we provided logistical support for two scientists (R. Bindschadler and J. Foster) from the Goddard Space Flight Center in Greenbelt, Maryland who collected field data on snow levels and snow moisture content on some of the alpine glaciers in the field area. They planned to try to correlate this data with TM data collected during the same

period. The long term objective of this project is to allow glacial snow budgets to be evaluated by TM data. This project is being carried out in cooperation with Dr. Dorothy Hall of the Goddard Space Flight Center in Greenbelt, Maryland. We also provided logistical support to Marc Hirschmann, a Masters degree candidate from the University of Oregon, who was studying granophyric dikes and sills in the Skaergaard intrusion. Mr. Hirschmann's thesis was indirectly supported by this project but is not included with the list of "Student Theses resulting from NAS 5-28738" (Hirschmann, Marc M., 1988, Petrology of the Transgressive Granophyres from the Skaergaard intrusion, East Greenland, MS Thesis, The University of Oregon, Eugene, OR).

Additional field observations were made during July and August of 1988 by the PI with the goal of making on-site observations in areas where the TM images gave contradictory information, and obtaining more field data on the nature and distribution of surface stains and lichen cover in the field area. In addition, a number of oriented samples from the Skaergaard, Basistoppen, and Vandfaldsdalen intrusions were collected for petrofabric studies to determine the extent of preferred mineral alignments within these intrusions. Such preferred mineral orientations may result in increased specular reflection on some outcrop surfaces. The nature of mineral alignments in these rocks is also of interest because of its potential for providing insights into the crystallization processes responsible for the present distribution of chemical constituents. The 1988 expedition included Dr. H. Richard Naslund and Brian W. Stewart, a PhD candidate at The University of California at Los Angeles. Mr. Stewart's PhD Dissertation,

which will be completed in the Fall of 1989, was indirectly supported by this project but is not included in the list of "Student Theses resulting from NAS 5-28738".

Laboratory Research

Laboratory research for this project included image processing of TM data under the direction of J. T. Parr at TASC, and processing of HHRR and topographic data under the direction of R. W. Birnie at Dartmouth College. The details of the image processing are presented in the following section of this report (Digital Processing of Thematic Mapper Imagery) and selected images are presented in appendices 3 (TM Imagery of the Skaergaard intrusive center) and 4 (TM Imagery of the Kangerdlugssuaq, Kap Edvard Holm, Gardiner, Kruuse Fjord, Imilik, Borgetinderne, and Lilloise intrusive centers). The results of the HHRR study are presented in appendices 1 (Applications of Landsat Thematic Mapper and Ground Based Spectrometer Data to a Study of the Mafic Intrusions of East Greenland) and 2 (Calibration of Fibrefrax Standard and Effect of Different Illumination Angles). The correlation between topography and TM data in the Western part of the Skaergaard intrusion was investigated by M. K. Cobb and formed the basis for his Batchelors thesis at Dartmouth College (Analysis of the Topographic Effects on Landsat Spectral Brightness: Kraemer Island, Skaergaard Intrusion, East Greenland).

Digital Processing of Thematic Mapper Imagery

Processing Environment and Objectives.

All digital image processing for this study was accomplished by The Analytic Sciences Corporation (TASC) using the resources of its Computing Technology Center (CTC). At the initiation of the program, the image processing facilities were hosted on a DEC VAX 11-785. During the course of this effort that equipment was upgraded. All image processing results presented within this document were prepared using the new configuration, comprising (in part) an Alliant FX/8 mini-supercomputer and a Gould/DeAnza Model IP-8500 image processor. This sytem operates under Alliant Concentrix (a UNIX-like operating system). The image processing software used is part of the TASC Interactive Image Processing System (TIIPS), a C language based package of algorithms developed by TASC. Fortran subroutines are used within the more computationally intensive programs to take advantage of the Alliant's parallel architecture.

TASC's role in this study was to utilize its imaging expertise and computer resources in the processing and enhancement of the Landsat Thematic Mapper (TM) imagery. Initially, the TM data was processed to provide base maps for use in the field portion of the study. Preliminary enhancements and attempts at lithologic classification were also made for use during the second field season (1986). This report discusses the final image processing results. These include various efforts aimed at lithologic discrimination and classification of units in the vicinity of the Skaergaard test area, and a

preliminary effort at discrimination of units around seven other Tertiary intrusions in East Greenland.

Imagery of Skaergaard and Vicinity

For ease of interpretation by field personnel, some of whom had minimal backgrounds in remote-sensing, a basic false color band composite image was used as the standard reference for imagery developed for use as base maps in the field. For this purpose, composites were generated using TM band 2 (blue), band 3 (green), and band 4 (red). The bands were each interactively enhanced using an interactive, non-linear (piecewise linear) contrast stretch to optimize discrimination of the regional geology. Band 1 was used minimally in this study due to the frequent saturation of the detector on the abundant snowcover, and the time dependent biases resulting therefrom. While this band combination is sufficient to distinguish the gabbro at Skaergaard from the adjacent Precambrian gneiss, it enables little other lithologic discrimination.

In an effort to distinguish variations within the gabbro and other units, a variety of band enhancements and band composites were evaluated. As noted above, band 1 tended to be rather noisy in this environment, and bands 1 and 2 were very highly correlated. Additionally, bands 5 and 7 were also highly correlated. A band 5/7 ratio had esentially no variance for areas of geologic interest. The best band composites for the Skaergaard area were generated using band 3 (blue), band 4 (green), and band 5 (red). These enabled both discrimination of the gabbro, gneiss, and basalt, as well as the

definition of some stucture with each of these units. The success of this band combination was, however, highly dependent on the use of the interactive contrast stretch. Because of the low reflectance of the gabbro and basalt, variations within these units are expressed as only a few gray levels. The sensitivity of a good interactive tool is essential to the analysis of this data.

While preliminary evaluation was performed using imagery acquired during the summer of 1985, the results were not particularly satisfying. Snowcover that season was unusually high, and a failure in the Landsat data downlink precluded image collection after 13 August. Maximal snowmelt generally occurs in September. A tradeoff must be made between mimimizing the snowcover and acceptance of greater shadowing, since the sun elevation is steadily decreasing after the summer solstace. The latitude at Skaergaard is approximately 68 degrees north. In mid-August the apparent sun elevation is about 35 degrees, but by mid-September it is down to 25 degrees. Since local terrain relief is slighly in excess of 1000 meters, a serious compromise between shadowing and snowmelt must be made. Unfortunately, the snowcover during the 1986 season was again greater than normal for the region, so lower sun elevations became a fact in the TM acquisitions actually used for this study. The final evaluations of the Skaergaard locality were made using imagery from both 8 August 1985 and 13 September 1986.

Merging of Multi-Temporal TM Imagery

Since extensive snowcover was such a serious problem in the evaluation of the Skaergaard imagery, approaches employing multi-temporal coverage were investigated. The most significant problem presented by the snow was the partial coverage prevalent in so many of the TM pixels. This, of course, has the impact of contaminating the apparent spectral reflectance of such pixels. Since many of these contaminated pixels are not contiguous with pixels obviously containing snow, the real problem is simply one of recognition.

To mitigate this problem, the best images from each of the 1985 and 1986 seasons were co-registered using a standard polynomial warping algorithm. Then, using data from areas known (from field photography) to be snow free, a transform (lookup table) was designed to effect a radiometric balancing of the 1986 image to the 1985 scene. This was done independently for each of the spectral bands, using control areas with a broad diversity in spectral characteristics. Once this transformation was accomplished the two scenes were compared on a pixel by pixel basis, again for each TM band. For bands 1-4, the assumption was made that as subpixel snowcover was reduced, the apparent brightness would decrease; therefore, a merged image was created using the lesser of the reflectances from the 1985 and the radiometrically balanced and co-registered 1986 data. Since snow is non-reflective in the short wave infrared, the brightening was assumed to imply reduced snowcover and the greater of the two

reflectances was used in the construction of the merged images for bands 5 and 7. Because of wind, terrain relief, and running water over many surfaces, the thermal infrared data were not found to be useful to this study, and no further processing of band 6 data was undertaken.

It is recognized that the assumed associations of pixel reflectance with snowcover are not exclusively true. The changes in solar azimuth and elevation also produce changes in shadowing. The impact of direct shadows is obvious and can be accounted for during analysis of the imagery. More suble darkening of a surface due to surface roughness where the local solar grazing angle (relative to the actual terrain surface) is small is more problematic. In large measure this can be accounted for since the majority of areas impacted will be contiguous with regions in direct shadow. Any pixel can, however, be affected if the local roughness is sufficient. This will necessarily result in erroneous results from the merge process described above. Nevertheless, when viewed from a contextural perspective, the merged results appear to improve significantly the spatial coherency of the images and thus facilitate the geologic interpretation. These images were used for all subsequent studies of the immediate Skaergaard area.

Band Ratios Images

The calculation of band ratio images was motivated by two considerations. Perhaps most significant was the need to mitigate the lighting effects produced by the substantial terrain relief and

subsequent variations in solar illumination of the surface. Of nearly equal interest, however, was the desire to enhance the effects of iron oxide and any hydroxyl absorption, and to test the band 5/1 ratio as an indicator of magnetite abundance. In addition, as the Hand Held Ratioing Radiometer (HHRR) data became available after the 1986 field season, the importance of both lichen coatings and surface mineral staining were better defined. Both of these surface coatings tended to overwelm the subtle spectal differences among the various units within the Skaergaard gabbro. As suggested by the HHRR data, band 5/3, 4/3, and 3/1 ratios were also calculated.

All band ratio images were derived from the raw TM data and subsequently scaled (linear clip and stretch) so as to maximize the discrimination of lithologic units. Presentation of that data with this report is in two basic formats. The first is a pseudocolor version of the stretched ratio images, where a low ratio appears blue in the image and a high ratio red; intermediate values change hue continuously through the visible spectrum. The second format is the band ratio composite, where each band ratio being used is assigned one of the three primary colors (red, green, or blue). In this format high ratio values contribute a larger fraction (intensity) of that hue to the composite image; hence, if the ratio represented by green has a very low value, green will be absent in the composite, resulting in a blue-magenta-red hue. In order to improve lithologic discrimination, all ratio composite images have been contrast stretched by individual band ratio, using the non-linear interactive tool previously noted.

Other Image Enhancement Techniques Employed

Intensity-hue-saturation (IHS) transforms were also used in an effort to improve discrimination of the subtle lithologic differences among the Skaergaard units. The IHS technique was chosen to enhance the minor variations in hue which were manifested within the gabbroic units using both band and band ratio composites. This was accomplished primarily by an interactive contrast stretch in hue space. Additional benefits were derived by compressing intensity space so as to mitigate the distracting effects of dark shadow and very bright snow and ice surfaces. Improvement was also achieved by stretching in saturation space; the band ratio data associated with shadow, snow, ice, and water were decolored, while the saturation levels associated with the lithologic units were increased. The combined effect of these changes, when the image was inverse transformed back into red-green-blue space, was to improve the interpretability of the imagery.

A final enhancement technique employed with the Skaergaard imagery involved the use of a principal component transformation. Since the image variance associated with snow, ice, water, and shadow is of little interest to the geologist, a multi-band synthetic image was first created by aggregating small patches of imagery, each of which was essentially free of the undesired factors. The patches were chosen from various sites around the Skaergaard area so as to obtain a reasonable distribution of lithologies. A covariance matrix was then computed from this TM image subset and applied to the full Skaergaard subscene. The resulting principal component images were then

evaluated, principal components 1, 2, and 4 appearing to contain the greatest lithologic information. A band composite image was created with these, along with an alternative presentation using highly non-linear, negative stretches of these same principal component images.

Classification of Skaergaard Imagery

Early in the study a supervised maximum likelihood classification of the August 1985 imagery of Skaergaard was attempted. Training cells for all major lithologic units as well as the various subunits within the Skaergaard intrusion were defined along with cells used to define snow, ice, seawater, turbid water, ponds, and shadow. No significant vegetation (except lichen and moss cover) exists in this region. The classification was highly confused, with even the major lithologic units being poorly defined. As previously reported, field work at Skaergaard has now identified several factors responsible for this inability to discriminate successfully. Perhaps most significant was the abundance on subpixel scale snowcover. Also important is the extensive lichen and mineral coating found, especially with the gabbroic units; thus far there has been no totally consistent pattern discerned which associates these coatings with any particular rock chemistry or lithology. Another factor of significance is specular reflectance. The combination of low sun elevations and the preferred dip slope orientation of the layered series in the gabbro yields a bias toward the specular component being detected by Landsat. The abundant magnetite alteration, glacial polish, and thin sheets of

water from snowmelt all were found to result in specular returns six to ten times brighter than the diffuse component. The color shift associated with these specular returns, though not quantified, was readily discernable in the field by eye.

Given the minor differences in the composition and the measured HHRR spectra for the gabbroic subunits, confusion within the intrusion was not surprising. Subsequent classification efforts were aimed primarily at an improved discrimination of the basic lithologies - the gneiss, gabbro, and basalt. To mitigate the snowcover issue, further evaluations were based upon the multi-temporal merged data set. New training cells were chosen, based upon field observations and photography, so as to better define representative, snow-free pixels.

A maximum likelihood classification was run, using training classes for the full set of non-lithologic categories along with classes for the gabbro (as a whole), the Basistoppen sill, the gneiss, and the basalt. The result was improved relative to the initial, preliminary study; but the large number of classes still resulted in a significant degree of confusion, manifested as a lack of spatial coherency. Identification of the Basistoppen was particularly poor, often being confused with the gneiss.

In an effort to improve these results, the non-lithologic classes were aggregated into a unifed snow-ice, (all) water, and shadow-morraine categories. The Basistoppen was eliminated, but the Skaergaard was divided into five subunits (Lower Zone 1, Lower Zone 2, Middle Zone, Upper Zone 1, and Upper Zone 2). Divergence statistics (based upon training cell covariance) predicted reasonable success in

discriminating the basic lithologic units, but little success in separating any of the gabbroic units (except minor success with the Middle Zone). The actual classification upheld these expectations. The gabbro and gneiss were reasonably well discriminated (in comparison with field mapping). The basalt to the southeast was identified along with an anomalous area on Kraemers Island (known amphibolites). Within the Skaergaard no discrimination was perceived except for perhaps 10-20 pixels of Middle Zone which were correctly identified. To eliminate some of the statistical noise prevalent in this classification, a 3 by 3 pixel median filter was then used to produce an image with somewhat higher spatial coherency. This image represents the most successful effort to date in using Landsat TM imagery to discriminate the lithologic units in the vicinity of Skaergaard.

A clustering algorithm was used in a final attempt to discriminate gabbroic subunits. Using the training cells previously identified, statistics were compiled using the band 3/1, band 5/3, and 5/1 ratios. The algorithm was run in an attempt to further split the gabbroic unit. Convergence was never achieved by the algorithm, again indicating the spectral similarity of the subunits. Though the matter has not been thoroughly analyzed, it is suspected that sensor quantization error may be a limiting factor in the discrimination of these very dark mafic and ultramafic units.

Imagery of Other East Greenland Intrusives

The original objective was to extend the classification results from Skaergaard to other known intrusive bodies in the East Greenland region. Since the only success in classification of the Skaergaard imagery came through the merging of multi-temporal data, classification of the other intrusions was precluded (no appropriate 1985 data had been obtained due to the Landsat downlink failure). It was subsequently decided to examine the September 1986 data. Both band 2, 3, 4 (blue, green, and red) and band 3, 4, 5 (blue, green, red) color composites were generated for each of the seven intrusives of interest.

The plutons examined were (from southwest to northeast) Imilik, Kruse Fjord, Kap Edvard Holm, Kangerdlugssuaq, Gardiner, Lilloise, and Borgtinderne. The scales used for these images varied from 40-120 meters per pixel according to the dimension of the individual pluton. Full resolution (30 meter per pixel) subscenes were also created for selected portions of each of these bodies. The band 3, 4, 5 color composites were generally the most effective for discrimination of basic lithologies. Differences were, however, often subtle, requiring careful application of the interactive contrast stretching tool. With this particular band combination, the intrusives generally appear more tan to brownish than the brighter orange of the surrounding gneisses. The basalts take on a somewhat greener hue, while syenites appear redder if a little less bright than the gneisses. It should be noted that, as is so often the case, these differences, while apparent on a digital display, are difficult to preserve in second generation photography.

Mineral Resourse Evaluation

In addition to developing a set of criteria for using TM data to recognize the various rock types associated with mafic intrusions in East Greenland, a major goal of this project is to evaluate the resource potential of mafic intrusions in East Greenland, and in continental rifting environments in general. Our field mapping of the distribution of sulfides in the Skaergaard intrusion has resulted in the location of a potential Pd/Pt/Au ore horizon. Layered tholeiitic intrusions are the primary sources of Pt and Pd, two strategic metals for which South Africa and the Soviet Union are the principal producers and the United States and Japan are the largest consumers. The initial Skaergaard magma, as sampled at the chilled contacts of the intrusion, contained approximately 20 ppb Pt, 15-26 ppb Pd, and 4-10 ppb Au. During crystallization of the lower part of the intrusion the magma was not saturated in S, and as a result the early formed rocks contain only minor amounts of Pt, Pd, and Au sulfides. During crystallization of the Middle Zone, the magma became saturated in S and precipitated an immiscible sulfide liquid. As a result of the extremely high partitioning of precious metals into sulfide liquids, the initial sulfide precipitation scavanged the magma of precious metals and formed a horizon with total Pt, Pd, and Au in excess of 4 gms per ton, and average ratios of Pt-Pd-Au approximately 1-4-3. Rocks overlying the economic horizon contain negligable precious metal values, evidence of the effective removal of these components from the magma by the initial sulfide precipitation. Volume estimated for the Skaergaard intrusion (150 km^3) suggest a total original Pt content of $9x10^6$ kgs, a total Pd content of $9x10^6$ Kgs, and a total gold content of $3x10^6$ kgs. Approximately half of the original mass of

the intrusion has been removed by erosion. Estimates of the extent of the enriched horizon in the Middle Zone of the intrusion (1m x 30 km^2) suggest that $5x10^4$ kgs Pt, $2x10^5$ kgs Pd, and $1.5x10^5$ kgs Au may be concentrated in an ore horizon. Platinova Resources Ltd. of Toronto, Canada, which has the exploration license for East Greenland (issued by the Danish Government) is currently evaluating the economic potential of this deposit.

Other intrusions in the East Greenland Tertiary Igneous Province which contain rocks types similar to those in the Skaergaard intrusion include the Kap Edvard Holm, Kruuse Fjord, and Imilik plutons, the Basistoppen sill, and the Kraemers Island, Vandfalsdalen, and Miki's Fjord Macrodykes. The initial Pt, Pd, and Au contents of the magmas which formed these intrusions are likely to be similar to that of the Skaergaard, but it is not known if these intrusions reached saturation in a sulfide liquid to produce horizons with concentrations of precious metals. The areal extent of the Kap Edvard Holm intrusion is approximately 5x that of the Skaergaard and the areal extent of the Kruuse Fjord is more than 10x that of the Skaergaard. The presently exposed extent of the Imilik intrusion is approximately half that of the Skaergaard but the Imilik extends for an unknown distance below sea level. The areal extents of the Basistoppen sill and the associated macrodykes are significantly less than that of the Skaergaard intrusion.

Student Theses resulting from NAS 5-28738:

Brinkema, C. B., 1986, The Hammersdal Sill, Kangerdlugssuaq Region, East Greenland, BS thesis, Dartmouth College, Hanover NH.

Turner, P. A., 1986, The Sulfide Mineralogy and the Behavior of S and Certain Transition Elements in the Skaergaard Intrusion, East Greenland, MS

thesis, Dartmouth College, Hanover, NH.

Urquhart, J., 1986, Depth of Emplacement and Cooling History of the Skaergaard Intrusion, East Greenland as Revealed by Fission Track Dates, MS thesis, Dartmouth College, Hanover, NH.

Barnett, D. E., 1987, A Petrologic Study of the Kraemer Island Macrodike, East Greenland, MS thesis, Dartmouth College, Hanover, NH.

Nichols, J. D., 1987, A Ground Based and Landsat Spectral Study of the Skaer- gaard Intrusion, East Greenland, BS thesis, Dartmouth College, Hanover NH.

Cobb, M. K., 1987, Analysis of the Topographic Effects on Landsat Spectral Brightness: Kraemer Island, Skaergaard Intrusion, East Greenland, BS thesis, Dartmouth College, Hanover NH.

Keith, D. W., 1988, Observations on Layering in the Upper Border Series of the Skaergaard Intrusion, East Greenland, MS thesis, Dartmouth College, Hanover, NH.

Publications resulting from NAS 5-28738:

Naslund, H.R., Conrad, M.E., Urquhart, J. and Turner, P.A., 1986. Computer simulation of apparent grain sizes in thin sections - applications to grain size variation in the Skaergaard intrusion, EOS Trans. Amer. Geophys. Union 67, 384.

Turner, P.A., and Naslund, H.R., 1986, The mineralogy and distribution of sulfides in the Skaergaard intrusion, East Greenland, Geol. Soc. Amer. Abst. with Prog. 18, 776-777.

Turner, P.A., Naslund, H.R., and Keith, D.W., 1986, Observations on rhythmic layering in the middle zone of the Skaergaard intrusion, East Greenland,

Geol. Soc. Amer. Abst. with Prog. 18, 777.

Naslund, H.R., 1987, Lamellae of baddeleyite and Fe-Cr-spinel in ilmenite from the Basistoppen sill, East Greenland, Canadian Mineral. 25, 91-96.

Naslund, H.R., Parr, J.T., and Birnie, R.W., 1987, Lithologic mapping of mafic intrusions in East Greenland using Landsat thematic mapper data, Proceedings of the Third Annual Landsat Workshop, Laboratory for Terrestrial Physics, NASA, 157-162.

Barnett, D.E., and Naslund, H.R., 1987, A petrologic study of the Kraemer Island Macrodyke, East Greenland, Geol. Soc. Amer. Abst. with Prog. 19, 580.

Keith, D.W., and Naslund, H.R., 1987, Petrographic and chemical characteristics of a layered sequence in the Upper Border Zone of the Skaergaard intrusion, East Greenland, Geol. Soc. Amer. Abst. with Prog. 19, 723.

Turner, P.A., and Naslund, H.R., 1987, PGE abundance in the Skaergaard intrusion, East Greenland, Geol. Soc. Amer. Abst. with Prog. 19, 872.

Urquhart, J., and Naslund, H.R., 1988, Depth of emplacement for the Skaergaard intrusion, East Greenland as revealed by fission track dates, Geol. Soc. Amer. Abst. with Prog. 20, 77.

Parr, J.T., Birnie, R.W., Naslund, H.R., and Nichols, J.D., 1988, Lithologic mapping in East Greenland with Landsat thematic mapper imagery, Proceedings of the Sixth Thematic Conference on Remote Sensing for Exploration Geology, ERIM, Houston, Texas., 203-212.

Naslund, H.R., 1989, Petrology of the Basistoppen sill, East Greenland: A calculated magma differentiation trend, J. Petrol. 30, 301-321.

Birnie, R. W., Parr, J. T., Naslund, H. R., Nichols, J. D., and Turner, P. A., 1989,

Applications of Landsat Thematic Mapper and Ground Based Spectrometer Data to a Study of the Skaergaard and Other Mafic Intrusions of East Greenland, accepted for publicationin Remote Sensing of the Environment.

Naslund, H.R., ( ), Grain size variations in plutonic igneous rocks part 1: Theory, submitted to J. Petrol.

Naslund, H.R., Turner, P.A., and Keith, D.W., ( ), Crystallization and Layer Formation in the Middle Zone of the Skaergaard intrusion, submitted to Bull. Geol. Soc. Denmark.

Turner, P. A., and Naslund, H. R., ( ), Distribution of sulfides in the Skaergaard intrusion, East Greenland, IN PREPARATION.

Naslund, H. R., Birnie, R. W., and Parr, J. T., ( ), Geologic mapping in East Greenland using Landsat TM imagery, IN PREPARATION.

Appendix 1

Applications of Landsat Thematic Mapper and Ground Based Spectrometer Data to a Study of the Skaergaard and Other Mafic Intrusions of East Greenland

by

Richard W. Birnie (1), J. Thomas Parr (2), H. Richard Naslund (3), Jennifer D. Nichols (4), and Patricia A. Turner (5)

(1) Dartmouth College, Hanover, NH
(2) The Analytic Sciences Corporation, Reading, MA
(3) Dartmouth College, now at SUNY - Binghamton, Binghamton, NY
(4) Dartmouth College, now at Harvard University, Cambridge, MA
(5) Dartmouth College, now at Platinova Resources Ltd., Toronto, Canada

Submitted:
Remote Sensing of Environment
August 1988
(revised November 1988)

ABSTRACT

Landsat TM data have been used in conjunction with field spectrometer data to map the lithologic units associated with a series of gabbroic intrusions in the East Greenland Tertiary Igneous Province. The general lack and vegetation combined with the difficulty of access to these intrusions make them ideal candidates for lithologic mapping using remote sensing techniques. In addition, these bodies are of interest as possible precious metal ore deposits. The intrusions are spectrally distinct from the surrounding Precambrian gneisses; however, subpixel contamination by snow, oxide surface coatings, lichen cover and severe topography limit the discrimination of lithologic units within the gabbro. The spectral nature of the surface contaminants was evaluated with a Barringer Hand Held Ratioing Radiometer (HHRR). These HHRR data indicate that bare rock exposures have distinct TM signatures for each lithologic unit but that even small amounts of subpixel contamination are enough to mask these differences because of the large differences between the TM signatures of the rocks and the contaminants.

1. INTRODUCTION

A series of Tertiary plutons are exposed along 800 km of remote coastline in East Greenland. These plutons are correlated temporally and spatially with the initiation of Eocene rifting between North America and Europe. The focus of this study has been to determine the extent to which Landsat TM data can be used to locate the plutons and map lithologic variations in and around them. There is a particular interest in these plutons because they have the potential for gold, chromium, platinum, and palladium mineralization.

The study area extends along the central east coast of Greenland, approximately from Angmagssalik northward to Scoresby Sund (Fig. 1). The westward limit of the province is masked by the continental ice sheet. The well studied Skaergaard intrusion (Wager and Brown, 1967) is located near the center of the study area and serves as a control site for determining the Landsat TM spectral signatures of the various lithologic units. Thematic Mapper data were collected during the summers of 1985 and 1986, and field teams visited the Skaergaard area during both seasons. Some of the material included in this paper was presented at the 1988 ERIM Symposium (Parr et al., 1988) and some of the material is drawn from theses by Turner (1986) and Nichols (1987).

2. REGIONAL GEOLOGY

The rocks of the East Greenland Tertiary Igneous Province include layered tholeiitic gabbro plutons, sills, and macro-dikes; alkaline gabbro, syenite, and granite plutons; and tholeiitic flows, tuffs, and agglomerates, which form an 8 km thick sequence of flat lying plateau lavas. Most of the igneous activity occurred during the period from 60 to 50 m.y. ago (Brooks and Gleadow, 1977), when Greenland was rifted from northern Europe during the opening of the North Atlantic Ocean. The intrusive rocks in the province form a series of plutonic centers exposed along an 800 km long segment of the East Greenland coast (Fig. 1).

The Skaergaard complex is the most well-known of the intrusive centers (Figs. 2 and 3). It contains a central layered tholeiitic pluton, several associated layered tholeiitic macro-dikes and sills (e.g. the Basistoppen sill [Bs]), and numerous quartz and feldspar-rich granophyric bodies (Gs) ranging from dikes only centimeters wide to sills up to 100 meters thick. The central pluton, which is approximately 5 by 8 km in plan view, has undergone an extensive differentiation history from an initial Mg-rich to a final Fe-rich magma (Wager and Brown, 1967). This differentiation history is recorded in the rocks which crystallized on the floor (the Layered Series), the walls (the Marginal Border Series), and the roof (the Upper Border Series) of the magma chamber. A number of distinctive rock types were formed during this differentiation process, and include from the base of the intrusion upward (i.e. within the Layered Series): olivine-pyroxene-plagioclase gabbro (Lower Zone a+b, LZa+b); olivine-pyroxene-plagioclase-titanomagnetite gabbro (Lower Zone c, LZc); pyroxene-plagioclase-titanomagnetite gabbro (Middle Zone, MZ) fayalite-pyroxene-plagioclase-titanomagnetite gabbro (Upper Zone a, UZa); and fayalite-pyroxene-plagioclase-titanomagnetite-apatite gabbro (Upper Zone b+c, UZb+c). The units of the Marginal and Upper Border Series are in general coarser grained and texturally distinct from those of the Layered Series.

Subsequent to crystallization, the entire body was tilted about 20 degrees to the southeast. As a result, the present erosional surface exposes nearly the entire Layered Series and Upper Boarder Series from the base of the sequence in the northwest to the top of the sequence in the southeast. Dip slopes tend to become well-developed along some of the more plagioclase-rich bands, particularly in the MZ and UZa. The Skaergaard is bounded on the northwest by Precambrian gneiss (PCG), approximately 3 billion years old, and on the southeast by the Tertiary basalts, interbedded sills and agglomerates (Wager and Brown, 1967).

A number of other large plutons are recognized within the East Greenland Tertiary Igneous Province. Among these are the large Kangerdlugssuak and Kap Edvard Holm intrusions, both of which include gabbros and syenites (Fig. 1). The former is centered about 40 km west of the Skaergaard and is more than 25 km in diameter; the latter lies just south of the Kangerdlugssuak,

and is about 20 km in diameter.

Layered tholeiitic intrusions are the primary sources of chromium, platinum, and palladium, strategic metals for which South Africa and the Soviet Union are the principal producers, and the United States and Japan the largest consumers (Feichtinger et al., 1988). One aspect of this study was to determine possible Pt and Pd targets in the intrusions. To this end, a program for sampling and analysis of sulfide mineralization within the Skaergaard was conducted during the two field seasons.

The initial Skaergaard magma, as sampled at the chilled contacts of the intrusion, contained approximately 20 ppb Pt, 15-26 ppb Pd, and 4-10 ppb Au. These elements, however, are not uniformly distributed throughout the intrusion; they are less abundant in most of the sequence and are considerably more abundant in the Middle Zone (MZ). In the Skaergaard intrusion, the initial magma was not saturated in S, and, as a result, during the early stages of crystallization only minor amounts of S became trapped in the rocks formed by the magma. As crystallization proceeded, those elements which were excluded from the early-formed rocks became concentrated in the remaining magma. The Skaergaard magma reached saturation in S during crystallization of the MZ (Turner, 1986). When a silicate magma reaches saturation with respect to sulfur, any additional S is separated out as an immiscible sulfide liquid. Since sulfide liquids have strong affinities for precious metals, extremely high partitioning from the silicate melt can occur. In the Middle Zone, Pt, Pd, and Au were concentrated in excess of 4 gm/ton (4500 ppb). The average Pt-Pd-Au ratio is approximately 1-4-3. Rocks overlying the horizon high in precious metals contain negligible precious metal values, evidence of the very efficient removal of these components from the magma by the initial sulfide precipitation.

3. THEMATIC MAPPER DATA ANALYSIS

The first Landsat Thematic Mapper data for this study were obtained in July and early August, 1985 (Scene ID #'s 5052613102, 5052613104, and 5051013103) Field studies were undertaken during the data acquisition to develop a qualitative description of the various units which might be discriminated with the multi-spectral data. In addition, the area was well documented photographically; and distributions of snow, morainal material and glacial flour, vegetative cover, talus, and other transported debris were noted. Training areas for the various lithologic units in the region were also defined.

Transmitter problems aboard Landsat precluded any acquisitions after August 13 that year. This was particularly unfortunate since snowfall had been heavy, and much of the Skaergaard study area was still covered in early August. In 1986, there was also unusually heavy snowfall, but the impact on remote sensing was somewhat mitigated by data acquisitions (Scene ID #'s 5091713074, 509191255, 5092613011) later in the season (early September). However, the September data have the trade-off made with the use of the relatively low sun elevations (25°). The impact of this will be discussed in more detail later.

A dual approach was taken in the analysis of the TM data. Initially a number of standard image processing techniques were tested for their ability to aid in the discrimination of known lithologic units in the Skaergaard area. Interactive non-linear contrast stretch, band ratio color composites, principal component images, intensity-hue-saturation transforms, and adaptive enhancement algorithms were all evaluated with only partial success. While all techniques were moderately successful in separating the basic rock units (gabbro, gneiss, and basalt), no successful discrimination of the gabbroic sub-units within the Skaergaard intrusion was accomplished with any of these methods. An example of a principal components (PC) image is shown in Figure 4 (Scene ID # 5092613011). The airphoto shown in Figure 5 covers the central portion of the PC image. The geology of the area is shown in Figure 2. In the PC image, shadowed areas are green and snow, glacial ice and sea ice range from dark blue through light blue to cyan. The dark red areas generally represent the gabbro of the Skaergaard Intrusion shown particularly well in the region of the Skaergaard Peninsula below the center of the image. The N-S contact of the PreCambrian gneiss (light yellow) and the Skaergaard gabbros on

Kraemer Island is marked by an absence of yellow to the left (west) of the contact. This contact is shown in Figures 5 and 6. Areas of confusion occur in the central top and right top of the image where glacial moraine and Tertiary basalt, respectively, are imaged in red. The two photographs (Figs. 5 and 6) show the obvious contact of Precambrian gneiss (light colored) and Skaergaard intrusion (dark colored); however, even this clear contact is somewhat blurred by variations in reflectance presumably caused by subpixel snow, surface coatings, and topography that will be discussed in more detail later.

The second approach involved a maximum likelihood supervised classification. Training was based on pixels selected during the 1985 field study. Seventeen classes were defined, including all the gabbro sub-units, along with the gneiss, the Basistoppen Sill, granophyre sill, snow, sea ice, turbid water, ponds, seawater, and shadow; basalt was not present within the subscene being classified. The training cells were generally 300-500 pixels, but this number was not always achievable. For example, the Marginal Border Series has only about 20 pixels because of limited outcrop. The training cells included representative exposures of the various units with care taken to avoid an abundance of any particular illumination condition or geomorphic exposure. The signature means and covariance matrix for the training cells were evaluated using two measures: Bhattacharyya's distance and the closely related divergence, which are statistical measures of the spectral separability of training cells (Andrews, 1972, p.37-43; Tou and Gonzalez, 1974, p.291-307; and Moik, 1980, p.260-265). The signatures for gabbro, gneiss, and the two sills are reasonably distinct, giving generally estimated discrimination accuracies of 90-100 percent. (Tables 1 and 2). Of the gabbroic sub-units, only the UZa has a somewhat distinct signature. The mean signatures suggest, however, that much of the information on which the classification is based is albedo, rather than color. Therefore, classification accuracy is extremely sensitive to the problems of subpixel snow and local variations in illumination; and the actual classification is significantly confused by such factors. As with the initial image enhancement approach, the gabbro and gneiss were classified with moderate accuracy, but no coherent definition of the sub-units within the Skaergaard was achieved. Additional factors affecting classification accuracy are discussed in more detail later.

For the discrimination of the basic lithologies found in East Greenland, it should be noted that TM Band 1 data are particularly useful (Table 1). However, in this environment, Band 1 is often saturated by the snowcover. This introduces a time dependent, detector-related bias in the data. In many cases this bias precludes the use of Band 1 for the calculation of band ratios. The elimination of TM Band 1 from band ratios is particularly disappointing in light of the success reported by Sultan et al. (1987) for TM5:TM1 ratios in distinguishing relative amounts of magnetite and other opaque minerals in the hyperarid Eastern Desert of Egypt. Also, eliminating such band ratio data as a technique to mitigate the effects of terrain relief on local illumination, one is left with the option of deriving illumination corrections directly from digital terrain data. These data are not currently available, though they might be calculated from the stereo TM imagery available at this high latitude (68° N).

4. GROUND BASED SPECTROMETER STUDIES

Subsequent to difficulties experienced in classifying the Thematic Mapper data and in an effort to better understand the spectral properties of the various lithologic units, it was decided to collect field spectra during the second field season (August 1986). A Barringer Hand Held Ratioing Radiometer (HHRR) was used during the three week period from 4-25 August, 1986. This work is described in detail by Nichols (1987). The HHRR is a dual beam radiometer designed to measure the reflected radiance from a field target in any of ten user-selected bands. A set of switchable filters is used to collect data for all six of the Landsat TM visible and reflected infrared bands (here designated TM1, TM2, etc.). The reflected radiances were normalized by dividing by the reflected radiance of a Fiberfax standard. The HHRR was mounted one meter directly above the target on a standard camera tripod. At this working distance, the 2 by 12° field of view of the HHRR integrates the reflected radiance over a rectangular area about 3.5 by 21.0

cm. Measurements were taken only during cloudless days, generally between 9:00 and 15:00 local time. Sites were chosen with surfaces as nearly horizontal as possible.

Within each lithologic unit, at least three, and more typically six to ten, spectra were measured of exposed surfaces, with no inorganic or organic coatings. Having determined the spectral signature of the primary rock unit, attempts were made to measure the spectral variation due to surface coatings. These coatings included various inorganic stains, particularly red to black iron and manganese oxide stains, and various organic coatings, among them gray, black, orange, and red lichens, as well as less abundant mosses. These organic and inorganic components play a significant role in determining the spectral signature of lithologic units measured by the Thematic Mapper.

The mean HHRR spectral signatures of the fresh, non-coated rocks, plotted in ternary TM5-TM3-TM1 and TM4-TM3-TM1 spaces are shown in Figure 7-1 and 7-2, respectively. No organic or inorganic stains are affecting these signatures. Figure 7-1 shows that the major rock units, Precambrian gneiss, Tertiary basalt, and Skaergaard gabbros (LZa+b, LZc, MZ, and UZa), plot in unique regions in this ternary spectral space. This relationship is also preserved in TM7-TM3-TM1 ternary space, with the basalt more spectrally distinct from the gabbros. The spectral distinction between LZa+b (taken together as a single sub-unit) and LZc is minor in spite of the fact that LZc has about 20 modal percent titanomagnetite, while LZa+b have only about one modal percent titanomagnetite. In the field, LZc is dark brown, and LZa+b are light tan. The Upper and Middle Zones (UZa and MZ), ferrogabbro and gabbro, respectively, are spectrally distinct from the other units and from each other. They both contain about 15 modal percent titanomagnetite, but UZa contains olivine while MZ is olivine free. There is very little spectral distinction among the fresh, non-coated rock surfaces in TM4-TM3-TM1 space (Fig. 7-2). This emphasizes the importance of TM5 in separating these units. Within the Skaergaard gabbros, there is a progressive decrease in TM5 with increasing total iron content of the rocks.

The effects of varying degrees of inorganic mineral staining on fresh bare rock are best shown in TM5-TM3-TM1 spectral space (Fig. 7-1). Light to moderate degrees of staining cause a relative decrease in TM1, and with further staining there is a strong relative increase in TM5 and decrease in TM3. The change in TM4-TM3-TM1 space is less dramatic (Fig. 7-2), but increased mineral staining still results in a relative decrease in TM1 (with resulting increase in TM3 and TM4).

The influence of lichen shows up in both TM5-TM3-TM1 and TM4-TM3-TM1 spectral space (Fig. 7) with a significant increase in TM5 and TM4, relative to TM1 and TM3, as the organic cover increases. Mosses at Skaergaard exhibit similar spectral properties. The high TM4:TM3 values associated with increased lichen cover are consistent with the results of Ager and Milton (1987) who studied the effects of lichen on the spectral reflectance of granite, hornfels, and slate in the semiarid Extremadura region of Spain. Ager and Milton also note high TM5:TM2 values associated with certain lichens. This relationship also held with the Greenland lichen, but it was not as strong as the TM4:TM3 trend.

In addition to fresh rock surfaces being contaminated by varying degrees of vegetative and mineral coatings, small amounts of snow trapped in gullies and depressions also alter the spectra measured from the satellite. Patches of subpixel snow contaminate a significant fraction of the Skaergaard area pixels which are otherwise expected to be exposed rock. Examples of patches of subpixel snow can be seen in Figures 5 and 6. The TM5-TM3-TM1 and TM4-TM3-TM1 spectra of snow are shown in Figure 7. As expected, it is high in the visible and low in the reflected infrared bands. Each surface contaminant pulls the spectral signatures away from the pure exposed rock in a unique direction and causes extensive spectral overlap of otherwise distinct lithologic units.

5. FACTORS AFFECTING INTERPRETATION OF TM IMAGERY

Originally it was assumed that this part of Greenland was an ideal site to use remote sensing techniques for lithologic mapping. There are no trees or shrubs in the region and soil

cover is slight (Fig. 5). Given the difficult to nearly impossible access to most of the intrusions, the use of Thematic Mapper data seemed particularly appropriate. However, several factors have combined to make lithologic discrimination in this environment very difficult. These include snowcover, solar geometry, organic and inorganic coatings, and specular reflectance.

The TM data were collected in both 1985 and 1986 when the summertime snowcover was unusually extensive. While large parts of the Skaergaard area were exposed, the spatial frequency of subpixal snowcover was sufficiently high so as to influence the reflectance of many pixels. Field photography was used to eliminate from consideration some snow contaminated pixels within the training cells used for image classification, but all patches of subpixel snow could not be identified within the Skaergaard; and field access is not possible for the more remote intrusives.

Another significant factor influencing the interpretation of TM data in this region is the combined effect of organic and inorganic coatings. As shown with the HHRR data, the spectral variance due to these coatings is greater than that associated with the differences in lithology seen in the Skaergaard area. On the basis of field observations, there appears to be no correlation between lichen abundance and rock type, though there may be some correlation between abundance and solar exposure. This might provide some opportunity for increased classification accuracy if digital terrain data were incorporated. Mineral staining is much more pronounced within the gabbros, thus the ability to discriminate the major lithologic units is not totally compromised. Except for UZa, in which mineral staining is very well developed along widely exposed dip surfaces, mineral staining among the sub-units within the gabbro occurs with little regularity. This limits discrimination among the gabbroic subunits.

Several factors combine with topography and solar illumination geometry to create another adverse factor in image interpretation for this area. The combination of low sun elevations and the abundant southeast facing dip slopes results in a rather high specular contribution to the reflectance measured by Landsat. Several surface considerations make this important. Because of the abundant snowmelt occurring throughout the summer, reflection off wet rock surfaces is very common. In addition, the mineral stained dip surfaces noted above, especially in UZa, have an extremely high polish, and other surfaces have a high degree of glacial polish. Measurements in the field indicated that the specular component of reflectance from polished or wet surfaces is six to eight times greater than the diffuse component. Even relatively small, subpixel contributions from such sources are capable of masking the subtle differences among many of the lithologies.

A final factor influencing interpretation of the TM data is material mixing due to both downslope and glacial transport. Terrain relief in the Skaergaard area is approximately 1300 meters, and slopes are steep, ranging up to vertical and typically in the range of 25 to 45 degrees. At the lower elevations, gabbroic units from above are found well-mixed with those actually cropping out at the lower horizons. In addition, there are at least eight valley glaciers contributing to the transport of material over the intrusion; and much of the area was covered by continental glaciation during the last glacial advance. Throughout much of the region glaciation has left sizable moraines as well as thin, but more pervasive, coatings of glacial flour. Because of glacial transport, much of the flatter, more observable Skaergaard terrain contains numerous small gravel filled depressions with a rather heterogeneous mix of material, ranging from the abundant gneiss and basalt found nearby, to less common syenites and amphibolites. Clearly, these features pose serious difficulties to an accurate interpretation of the TM data.

6. CONCLUSIONS

Despite the paucity of major vegetation cover and the abundance of excellent rock exposure, it is clear that this high latitude, Arctic study site presents some very special challenges to the interpretation of remotely-sensed imagery. The problems include TM Band 1 saturation due to snow, subpixel contamination of lithologic signatures by mineral oxide coating and

organic lichen and moss, and steep topography resulting in areas of specular reflectance. These problems have precluded separating the various lithologic units within the overall gabbroic Skaergaard intrusion. However, the Skaergaard Intrusion itself and the other intrusions in the region can be clearly separated from the surrounding Precambrian gneiss based on their spectral signatures. This is particularly important in light of the potential for economic concentrations of Au-Pt-Pd in these intrusions and the possibility of further, yet undiscovered, intrusions of this nature in the Tertiary Igneous Province of East Greenland.

7. ACKNOWLEDGEMENTS

We wish to acknowledge and thank Barringer Limited, Rexdale, Ontario, Canada, for the loan of their Hand Held Ratioing Radiometer.

The work was primarily supported by NASA grant NAS 5-28738. Additional funds for field work in Greenland were provided by the Andrew K. Mellon and Richter Foundations and the Department of Earth Sciences, Dartmouth College.

Daniel E. Barnett, Corey B. Brinkema, Douglas W. Keith, Mathew K. Cobb, and Joanne Urquhart helped the authors during the field work.

8. REFERENCES

Ager, C. M. and Milton, N. M., 1987; Spectral reflectance of lichens and their effects on the reflectance of rock substrates: Geophysics, v. 52, p. 898-906.

Andrews, H.C., 1972, Introduction to Mathematical Techniques in Pattern recognition: Wiley - Interscience, 242 pp.

Brooks, C. K. and Gleadow, A. G. W., 1977; A fission-track age for the Skaergaard Intrusion and the age of the East Greenland Basalts: Geology, v. 5, pp. 539-540.

Deer, W. A., 1976; Tertiary igneous rocks between Scoresbysund and Kap Gustov Holm, East Greenland, in Escher, A. and Stuart, W. (eds.) Geology of Greenland: Geological Survey of Greenland, Kopenhaven, Denmark, p. 404-430.

Feichtinger, F., Lammer, A., and Riess, M., 1988; Platinum: the view from South Africa: Mining Engineering, v. 40, pp. 91-96.

Moik, J.G., 1980, Digital Processing of Remotely Sensed Images: NASA SP-431, 330 pp.

Naslund, H. R., 1984; Petrology of the Upper Border Series of the Skaergaard Intrusion: Journal of Petrology, v. 25, p. 185-212.

Nichols, J. D., 1987; A Ground Based and Landsat Spectral Study of the Skaergaard Intrusion, East Greenland: Undergraduate Honors Thesis, Dartmouth College, Hanover, NH, 63 pp.

Parr, J. T., Birnie, R. W., Naslund, H. R., Nichols, J. D., and Turner, P. A., 1988; Lithologic mapping in East Greenland with Landsat Thematic Mapper imagery: (in press) Sixth Thematic Conference, Remote Sensing for Exploration Geology, ERIM, Houston, TX, May 16-19, 1988.

Sultan, M., Arvidson, R. E., Sturchio, N. C., and Guinness, E. A., 1987; Lithologic mapping in arid regions with Landsat thematic mapper data: Meatig dome, Egypt: Geol. Soc. Am. Bull., v. 99, p. 748-762.

Tou, J.T. and Gonzalez, R.C., 1974, Pattern Recognition Principles: Addison-Wesley (Advanced Book program), 377 pp.

Turner, P. A., 1986; The sulfide mineralogy and the behavior of S and certain transition elements in the Skaergaard Intrusion, East Greenland: M.S. Thesis, Dartmouth College, Hanover, NH, 81 pp.

Wager, L. R., and Brown, G. M., 1967; Layered Igneous Rocks: W. H. Freeman and Co., San Francisco, 558 pp.

FIGURE CAPTIONS

Figure 1: Sketch map of the East Greenland coast between Angmagssalik and Scoresby Sund showing the approximate locations of the major intrusions (after Deer, 1976). The dark patches show the limit of exposed rock.

Figure 2: Geologic map of the Skaergaard Intrusion showing the distribution of the major subdivisions of the intrusion. Qgm = glacial moraine; Bs = post Skaergaard Basistoppen sill; UBS = Upper Border Series; MBS = marginal Border Series; LS = Layered Series; Tb = Tertiary basalts; Ks = Cretaceous sediments; PC = Precambrian gneiss (from Naslund, 1984).

Figure 3: Generalized east-west cross section of the Skaergaard intrusion.

Figure 4: Principal Components Image of Skaergaard Intrusion (Scene ID # 5092613011, 13 Sept. 1986). The image is approximately 10 km on a side. See text for discussion.

Figure 5: Air photo with north approximately up showing approximate N-S contact of Precambrian gneiss (light colored) and Skaergaard intrusion (dark colored) on Kraemer Island. Forbindelsesgletscher enters from the east on the right side of the photo. Uttental Sund separates Kraemer Island on the left from the mainland on the right. See Figure 2 for the geology.

Figure 6: View from Kraemer Island looking north across Uttental Sund showing contact of Precambrian gneiss (light colored) and Skaergaard intrusion (dark colored) on the Uttental Plateau.

Figure 7: Ternary diagrams of HHRR field data (7-1 is TM5-TM3-TM1 and 7-2 is TM4-TM3-TM1). Solid points are surface alteration (M1-moderate mineral stain, M2-heavy mineral stain, P1-moderate lichen cover, P2- heavy lichen cover, and S-snow). Open symbols are bare rock surfaces (1-gneiss, 2-LZa+LZb, 3-LZc, 4-MZ, 5-UZa, and 6-basalt). In Figure 7-2, points 1 and 6 are to the lower left, points 3 and 4 are to the top, and points 2 and 5 are to the lower right.

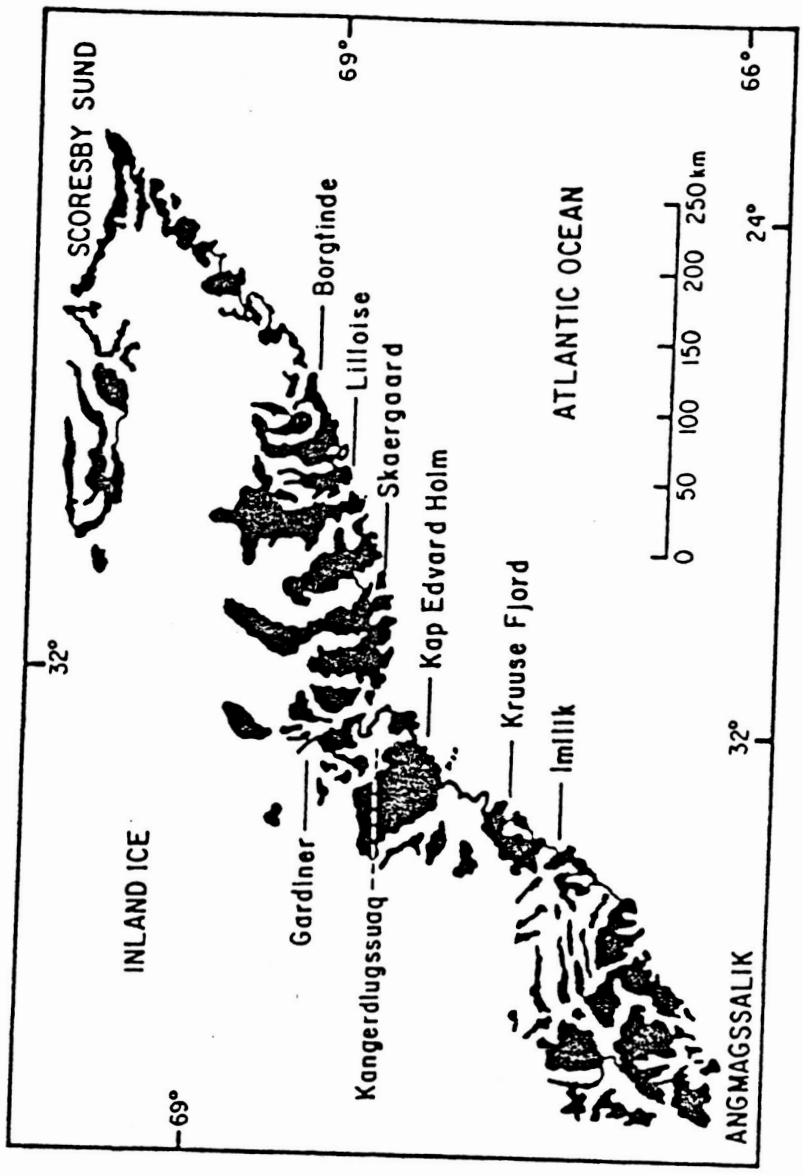
SCORESBY SUND
INLAND ICE
ATLANTIC OCEAN
ANGMAGSSALIK
Gardiner
Kangerdlugssuaq
Kap Edvard Holm
Kruuse Fjord
Imilik
Skaergaard
Lilloise
Borgtinde
69°
32°
66°
24°
0 50 100 150 200 250 km

Figure 1

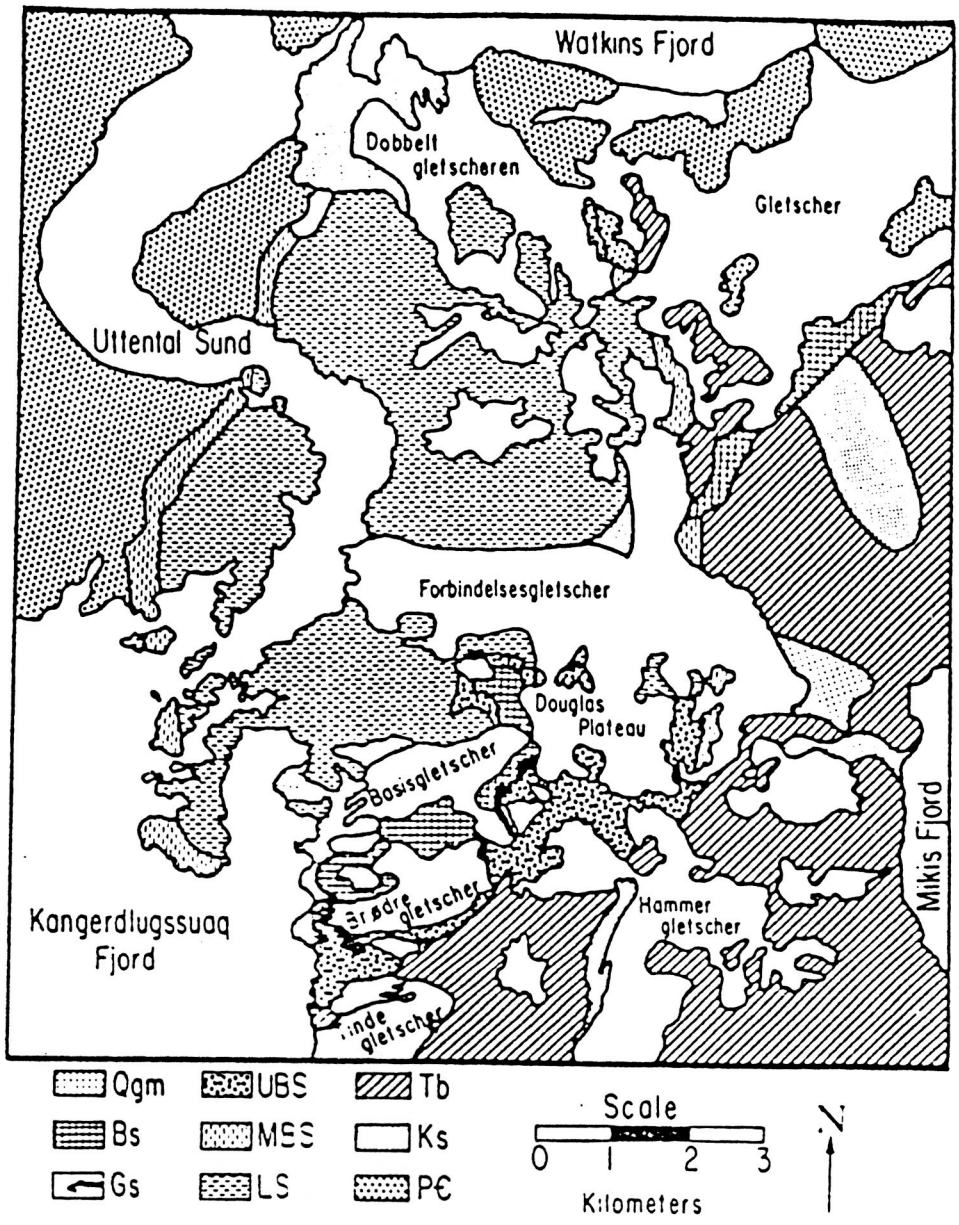
Watkins Fjord
Dobbelt gletscheren
Gletscher
Uttental Sund
Forbindelsesgletscher
Douglas Plateau
Basisgletscher
Mikis Fjord
Kangerdlugssuaq Fjord
Hammer gletscher
Qgm
UBS
Tb
Bs
MSS
Ks
Gs
LS
P€
Scale
0 1 2 3
Kilometers
N

Figure 2

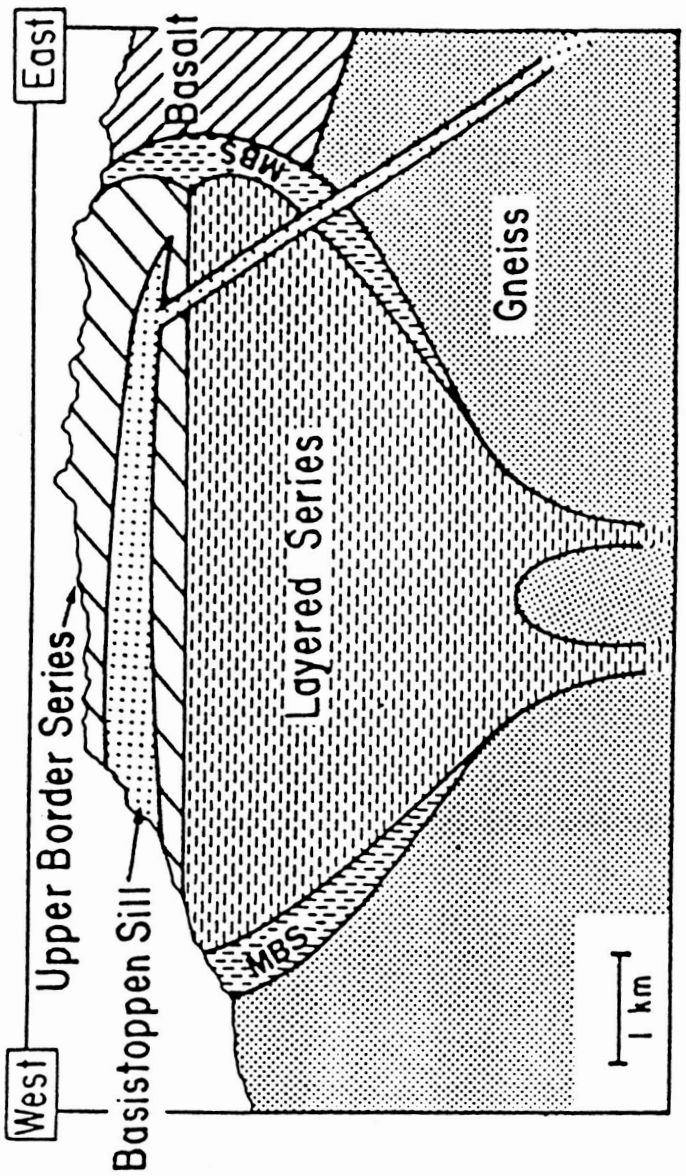
East
Basalt
SBS
Gneiss
Layered Series
Upper Border Series
Basistoppen Sill
MBS
1 km
West

Figure 3

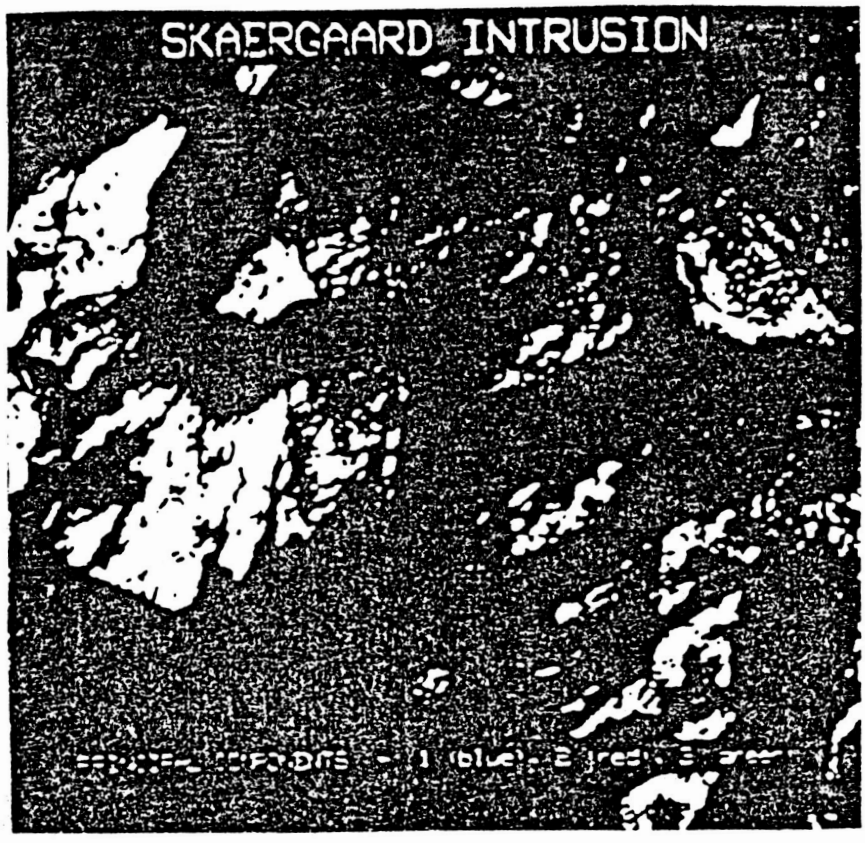

Figure 4

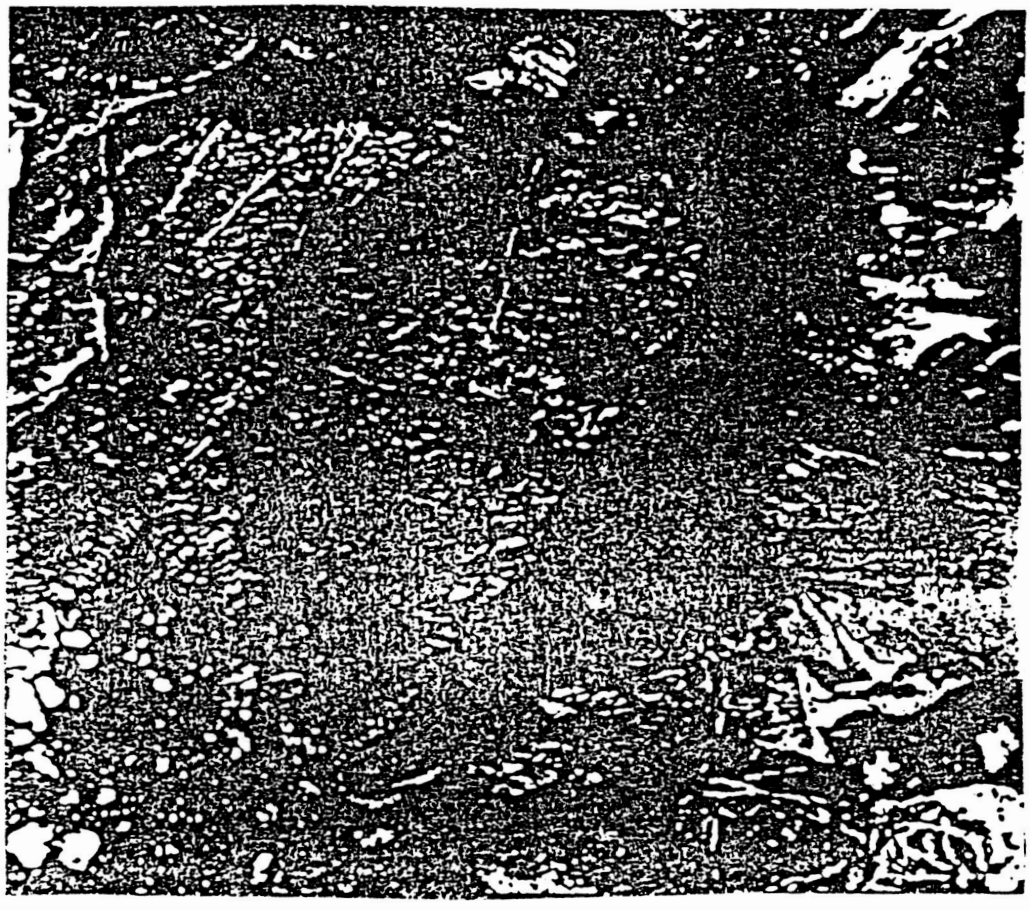

Figure 5

Figure 6

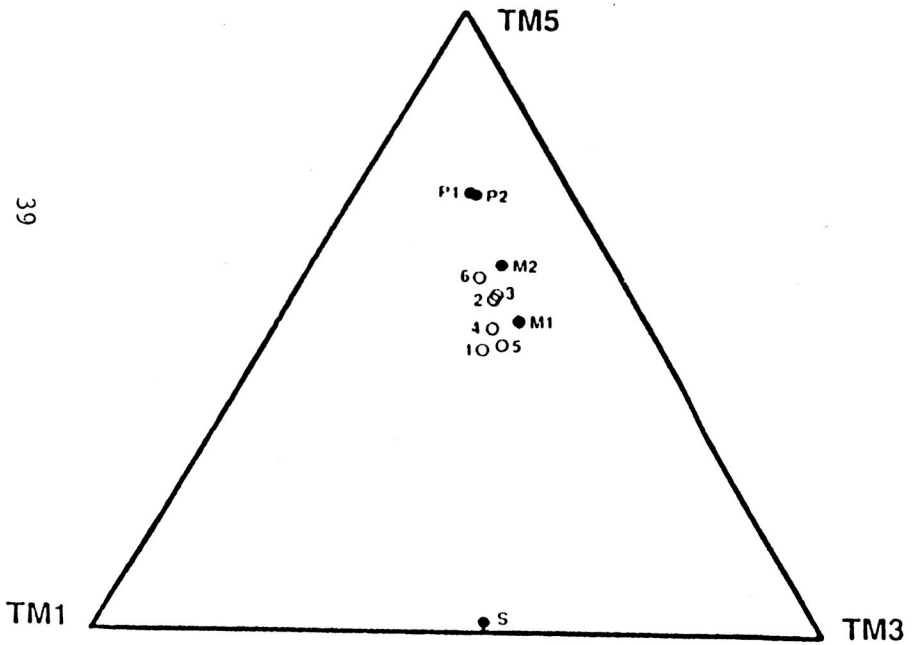

Fig 7-1

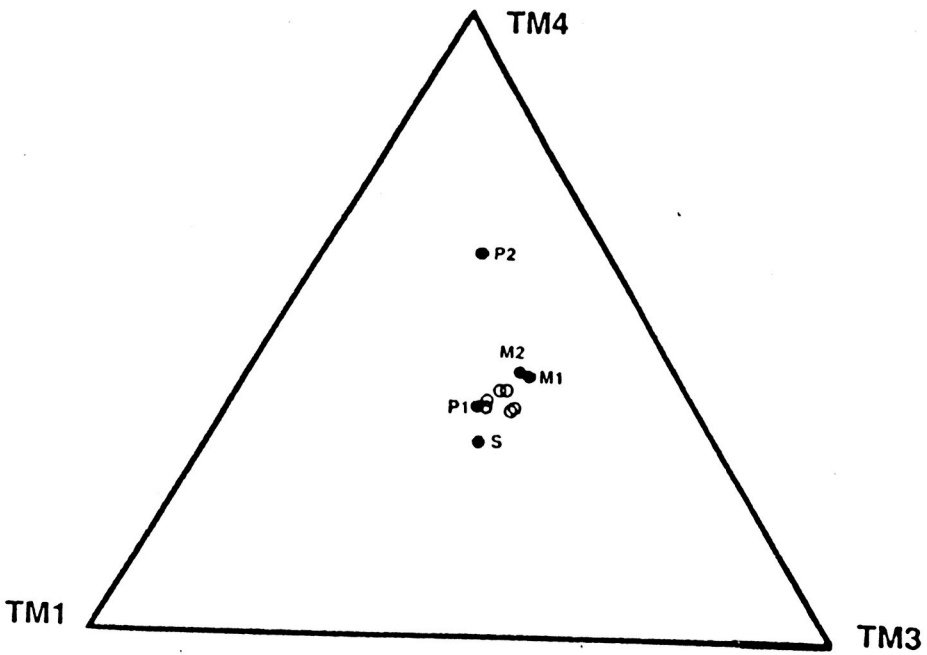

Fig 7-2

Table 1

TM SIGNATURES OF SKAERGAARD UNITS

(in Digital Numbers)

Lithologic Unit	1	2	3	4	5	7
Lower Zone a+b	117.2	48.5	59.9	43.9	67.8	40.9
Lower Zone c	119.0	48.1	59.3	42.1	60.0	35.7
Middle Zone	109.9	45.7	56.2	42.7	71.2	42.1
Upper Zone a	105.2	45.0	58.4	43.2	66.7	41.4
Upper Zone b+c	104.9	44.5	55.8	43.2	72.0	42.7
Basistoppen	119.7	49.3	62.5	46.6	87.8	53.3
Granophyre	113.4	49.1	64.9	50.9	105.2	62.6
pC Gneiss	130.4	55.6	70.3	53.1	101.4	61.4

Table 2

ESTIMATED CLASSIFICATION ACCURACY

(% BASED UPON TRAINING CELL STATISTICS)
(see text for unit abbreviations)

	LZa+b	LZc	MZ	UZa	UZb+c	Bs	Gs	PCG
LZ a+b	-	0	0	76	0	64	99	93
LZ c	0	-	0	70	0	100	100	100
MZ	0	0	-	55	5	100	94	94
UZ a	76	70	55	-	0	100	100	100
UZ b+c	0	0	5	0	-	98	54	88
Bs	64	100	100	100	98	-	66	0
Gs	99	100	94	100	54	66	-	99
PCG	93	100	94	100	88	0	99	-

Appendix 2

Calibration of Fibrefrax Standard and Effect of Different Illumination Angles

Because the ground based spectral measurements undertaken in the field with the Barringer Hand Held Rationing Radiometer (HHRR) were done at a generally low but also highly variable sun elevation angles (between at least 18 and 35°), we undertook an experiment to evaluate whether there is any specular component to the reflectance from fiberfrax standard. That is, does the color of the fiberfrax change with illumination angle.

An experiment was undertaken to examine the spectral reflectance properties of fiberfrax at illumination angles between 10° and 80° (Figure 1) A 90° (nadir) illumination angle was not possible because the illumination source interferrs with the spectroradiometer at that position (Figure 1). Data were collected in this experimental set up with both the high spectral resolution SE590 spectroradiometer (Table 1a) and the HHRR (Table 1b). Since only the HHRR was used in the field in Greenland, this analysis focuses on the HHRR data. The values in Table 1b are fiberfrax target signatures at various illumination angles (10°-70°) referenced against a fiberfrax standard at 80° illumination angle. Therefore, the illumination of the standard is held constant while the illumination of the target varies.

The results are plotted in Figures 2 and 3. Figure 2 shows that there is a steady decrease in reflectance with illumination angle. These would be predicted because as illumination angle gets lower, the cone of dispersion of the incident beam gets broader and, therefore, the intensity of illumination per unit of surface area drops. The drop off is predicted to be related to the sin of the illumination angle and that prediction is clearly supported in Figure 2 which includes a plot of the sin of the illumination angle with the spectral data. The reflectance values in Figure 2 converge to a value of 1.00 at 80° where the target and standard are both viewed at the same illumination angle. In Figure 2, the spectral characteristics of the standard are shown by plotting the six bands signatures at the different illumination angles. It can be seen clearly that there are now systematic changes in the color of the standard with illumination angle. There is some small random variability of the reflectance values, but no systematic change.

We next undertook an experiment to evaluate whether the reflectance properties of a rock might change under different illumination conditions. This experiment was undertaken with the exposed fresh surface of a large sample of gabbro from Greenland.

In this case, the data are measured and presented as standard field observations; that is, both target and standard are measured under the same illumination conditions.

The results listed in Table 2 and plotted in Figures 4 and 5. The TM band 1 values are not considered reliable because the incident illumination is low at those wavelengths and small percentage changes in instrument response will produce large changes in reflectance. Both Figures show that there is an increase in the reflectance values as the illumination angle gets lower. There appears to be little change in the relationship between bands at a given illumination angle, i.e. little difference in color; but there is a change in overall intensity. The systematic increase in reflectance with decreasing illumination angle is highlighted in Figure 6 with one band from the visible (TM 3) and one band from the near infrared (TM 5) plotted.

While the change in reflectance with illumination angle is systematic, the actual differences measured on both the target and standard are small. These values are plotted for both the gabbro and the fiberfrax for TM bands 3 and 5 in Figures 7 and 8 respectively. The general drop in reflectance signal with lowering illumination angle for the target and standard are shown clearly in these figures; the fibrefrax has already been shown to follow the sin curve (Figure 2). However, it is also clear from these figures (particularly Figure 8) that the gabbro does not fall off as rapidly as the fibrefrax. Therefore, when the reflectances are calculated by rationing gabbro to fibrefrax, the relative reflectances increase.

The reason for the increase at lower angles is not known, but it may be related to preferential orientation of feldspar cleavage faces. Since field measurements were taken under a variety of incident solar illumination angles varying between at least 18° and 35°, some variation in the overall brightness of our HHRR spectra are expected.

This change in reflectance is small relative to the differences seen in HHRR spectral signatures (Parr et al., 1988 and Birnie et al. in press) and would not effect the interpretations based on band ratios. However, this relationship may be critical in understanding reflected radiance differences seen in the satellite data. The step topograph and extreme illumination conditions in this artic environment provide a tremendous variation in surface plane to solar illumination direction.

Illumination Angle (ø)	sin(ø)	TM 1	TM 2	TM 3	TM 4	TM 5	TM 7
10	0.174	0.039	0.045	0.043	0.054	-	-
20	0.342	0.105	0.126	0.119	0.153	-	-
30	0.500	0.180	0.214	0.203	0.258	-	-
40	0.643	0.243	0.290	0.275	0.348	-	-
50	0.766	0.337	0.403	0.381	0.476	-	-
60	0.866	0.395	0.468	0.440	0.546	-	-
70	0.940	0.433	0.511	0.478	0.588	-	-

Table 1a. Simulated TM signatures of bands 1, 2, 3 and 4 for Fiberfrax reference standar calculated from SE590 spectra collected at different angles of illumination.

Illumination Angle (ø)	sin(ø)	TM 1	TM 2	TM 3	TM 4	TM 5	TM 7
10	0.174	0.073	0.078	0.076	0.079	0.079	0.090
20	0.342	0.255	0.253	0.243	0.253	0.252	0.276
30	0.500	0.391	0.380	0.362	0.380	0.380	0.409
40	0.643	0.550	0.535	0.527	0.544	0.545	0.581
50	0.766	0.700	0.671	0.671	0.684	0.688	0.725
60	0.866	0.818	0.797	0.800	0.802	0.813	0.800
70	0.940	0.900	0.887	0.887	0.892	0.892	0.896

Table 1b. Simulated TM signatures of bands 1, 2, 3, 4, 5 and 7 for Fiberfrax reference standard collected with HHRR at different angles of illumination.

Illumination Angle (ø)		TM 1	TM 2	TM 3	TM 4	TM 5	TM 7
10		29.63	20.87	22.81	23.90	45.29	54.33
20		14.81	16.60	18.18	19.08	38.76	45.32
30		15.31	15.34	16.40	17.32	36.02	42.57
40		10.00	14.03	15.08	16.02	33.84	40.10
50		12.64	13.57	14.64	15.65	33.02	39.19

Table 2. Laboratory reflectance spectra of gabbro under differing illumination conditions.

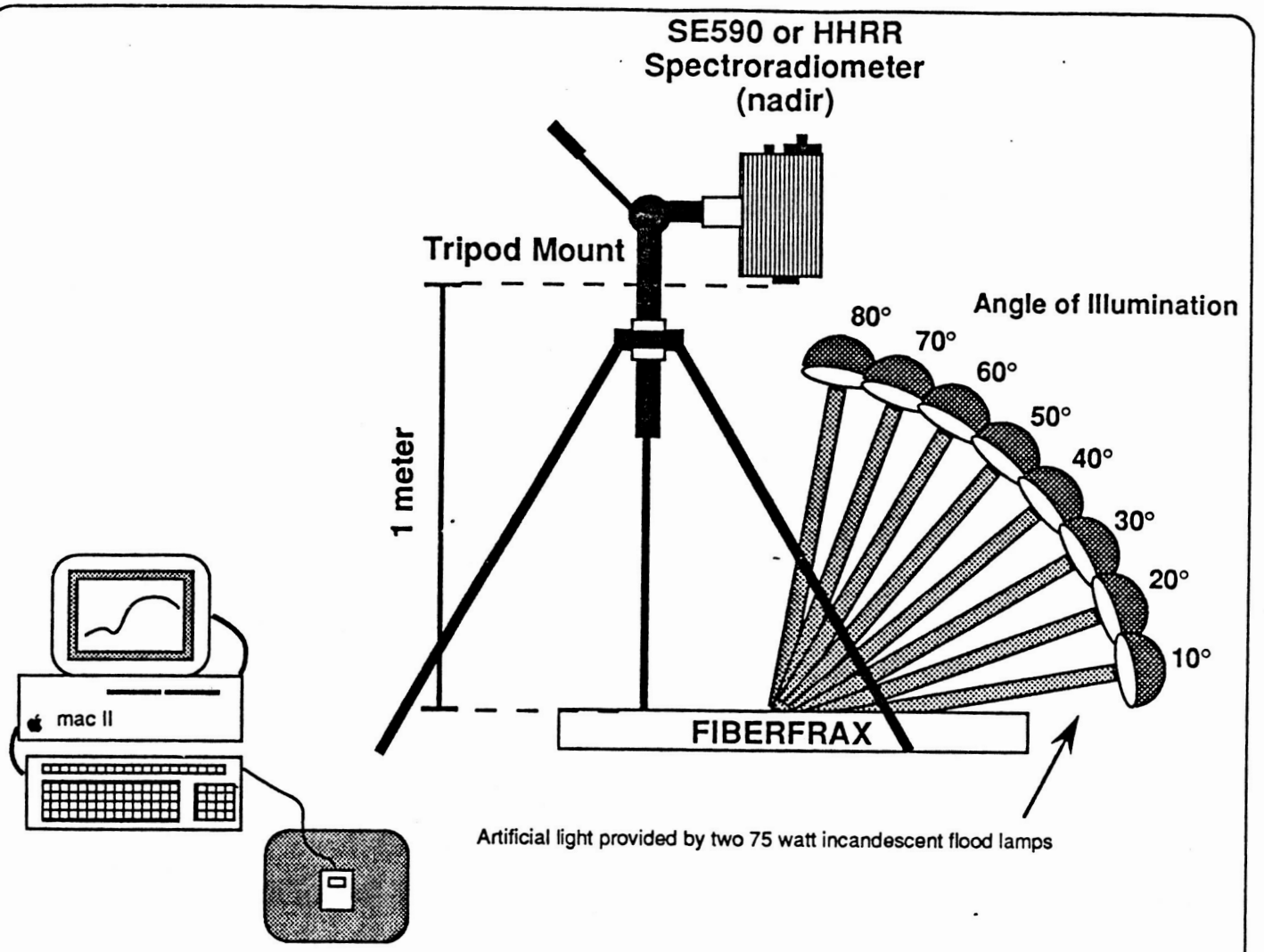

Figure 1. Laboratory set-up used for the analysis of Fiberfrax reflectance properties under differing illumination conditions. Measurements made with both the SE590 and HHRR spectroradiometers.

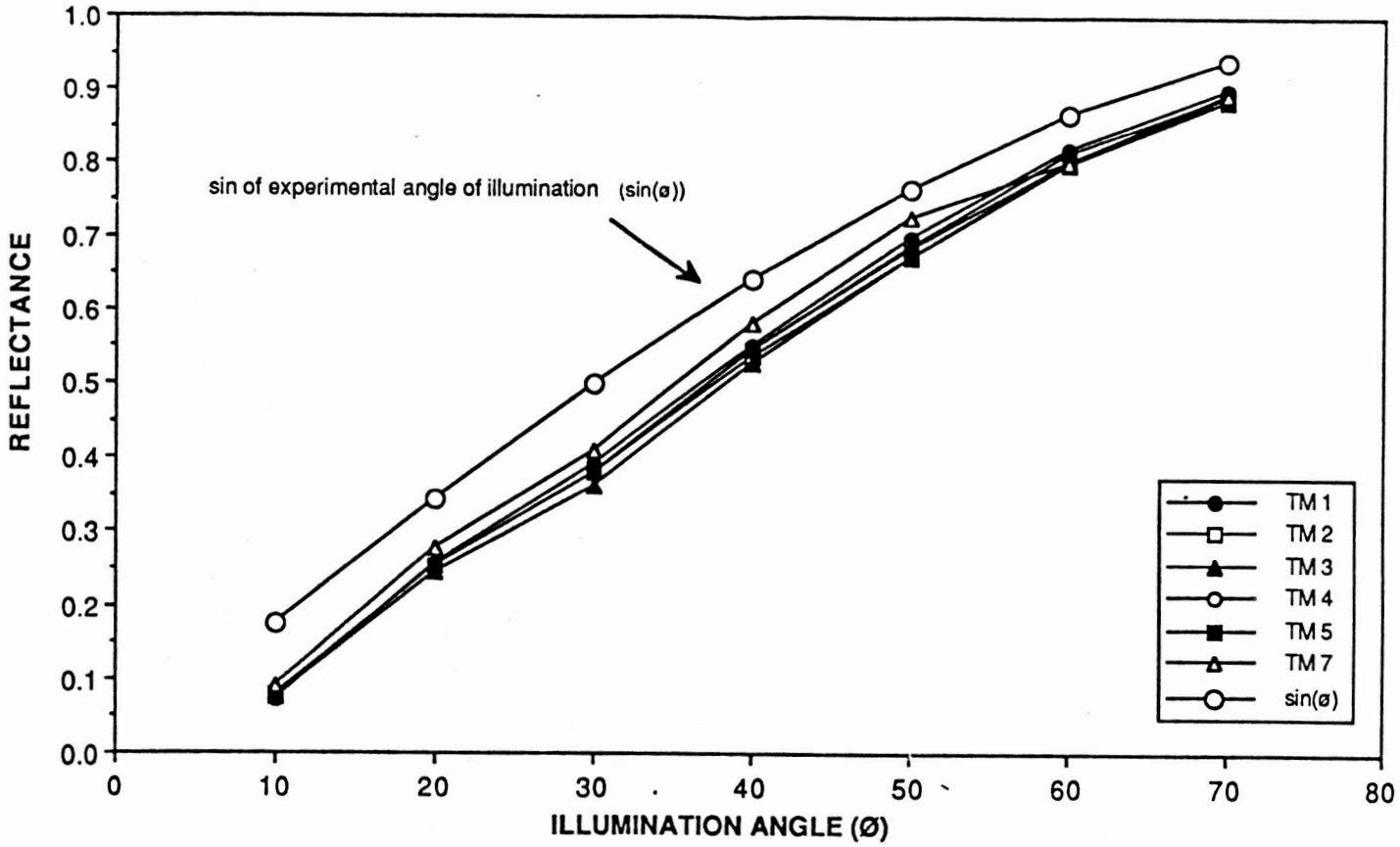

Figure 2

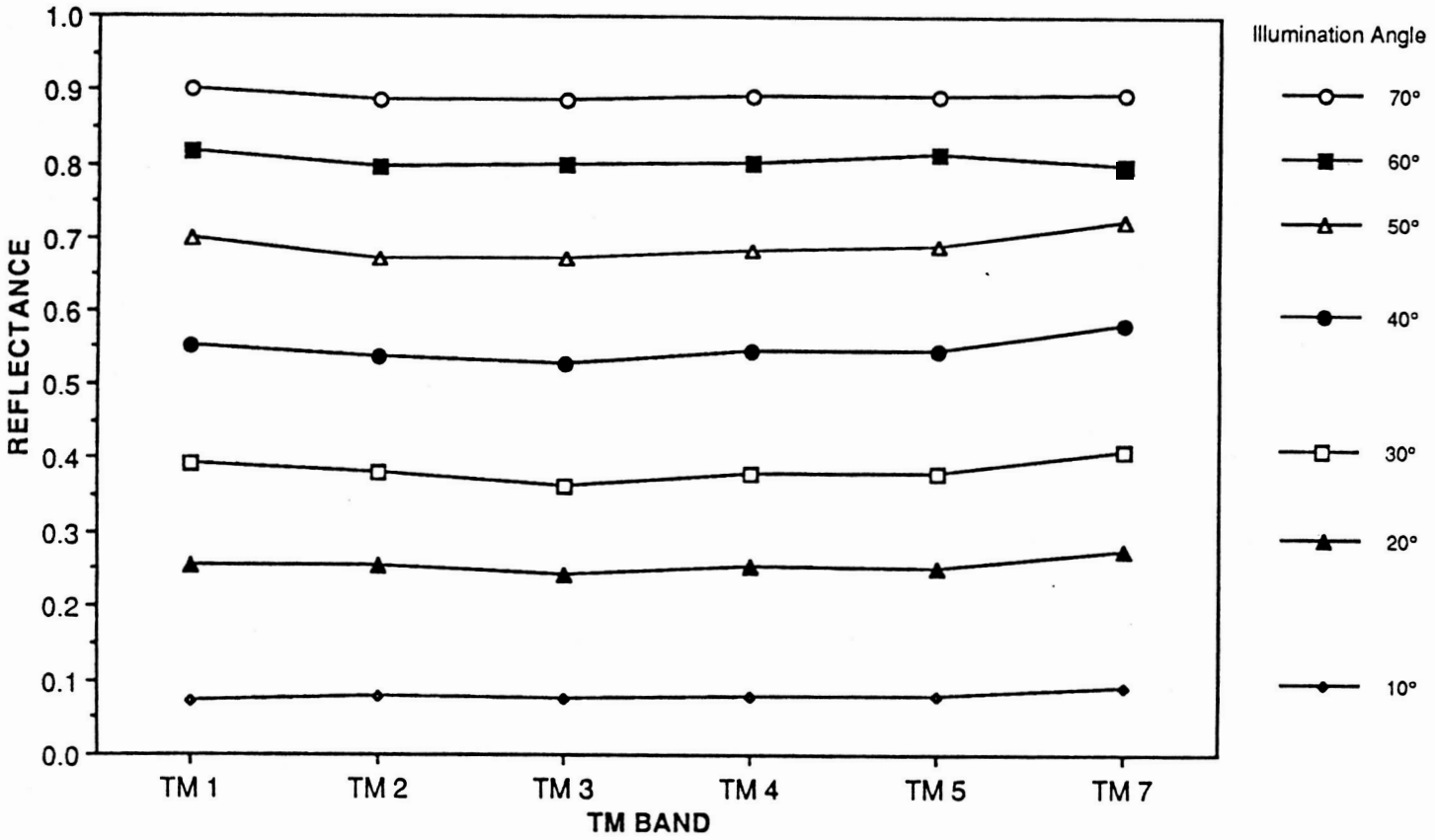

Figure 3

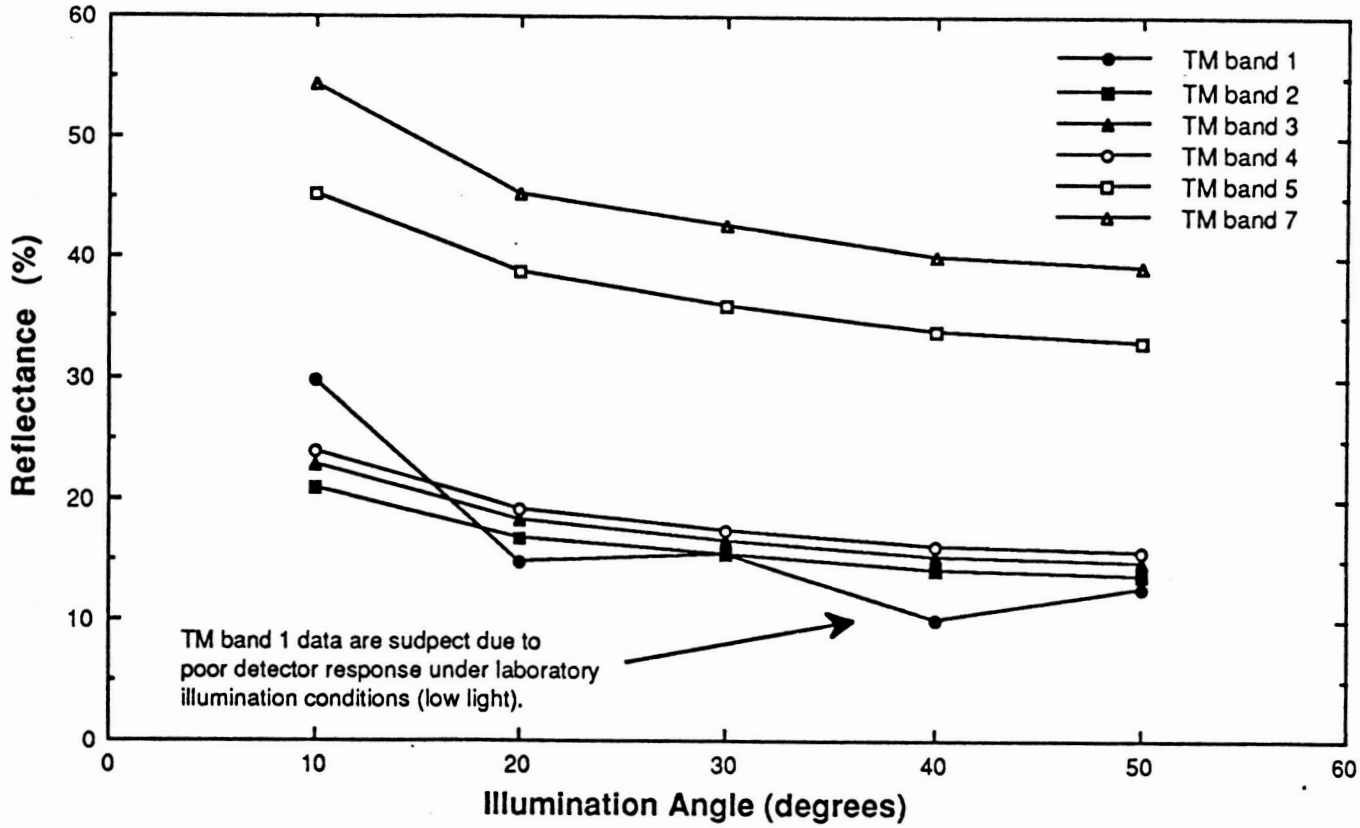

Figure 4.

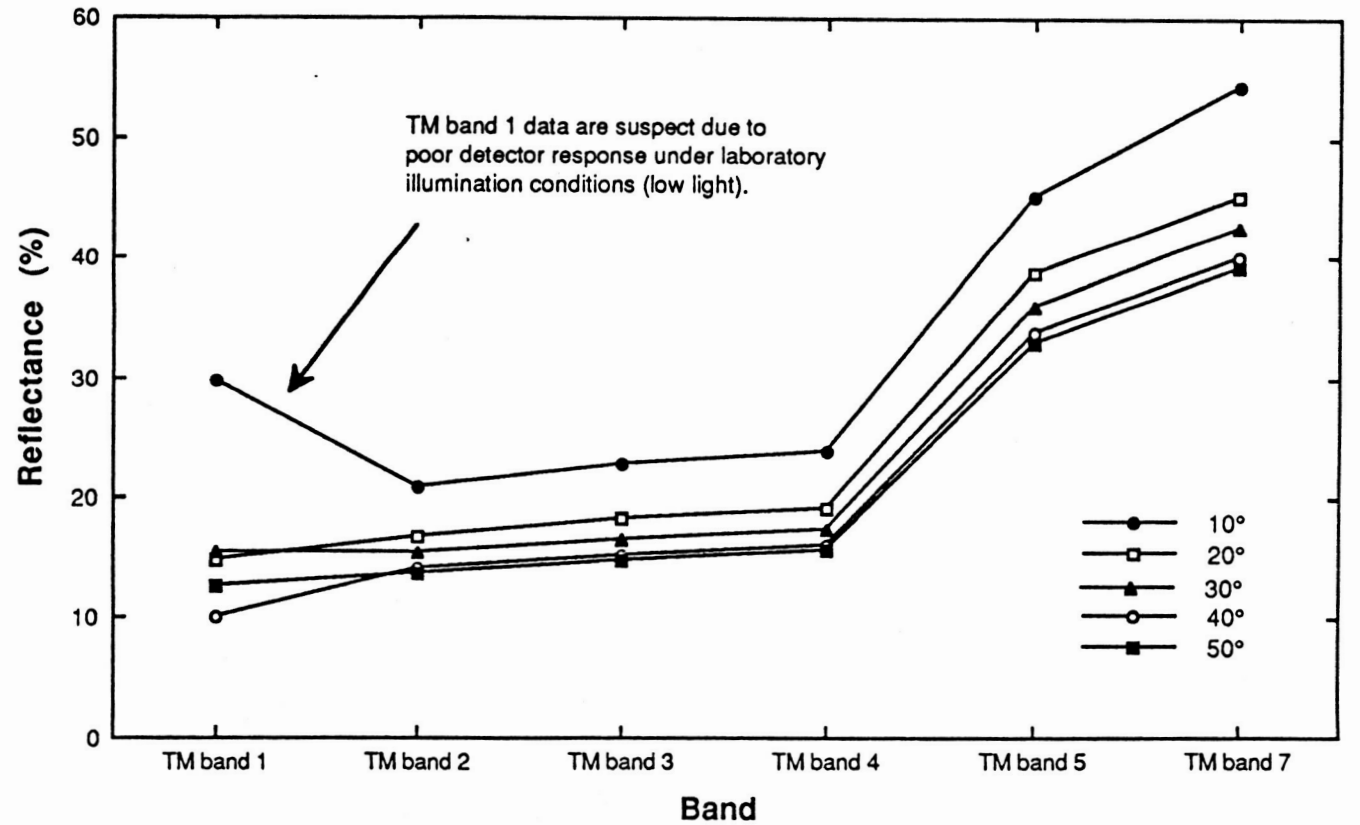

Figure 5.

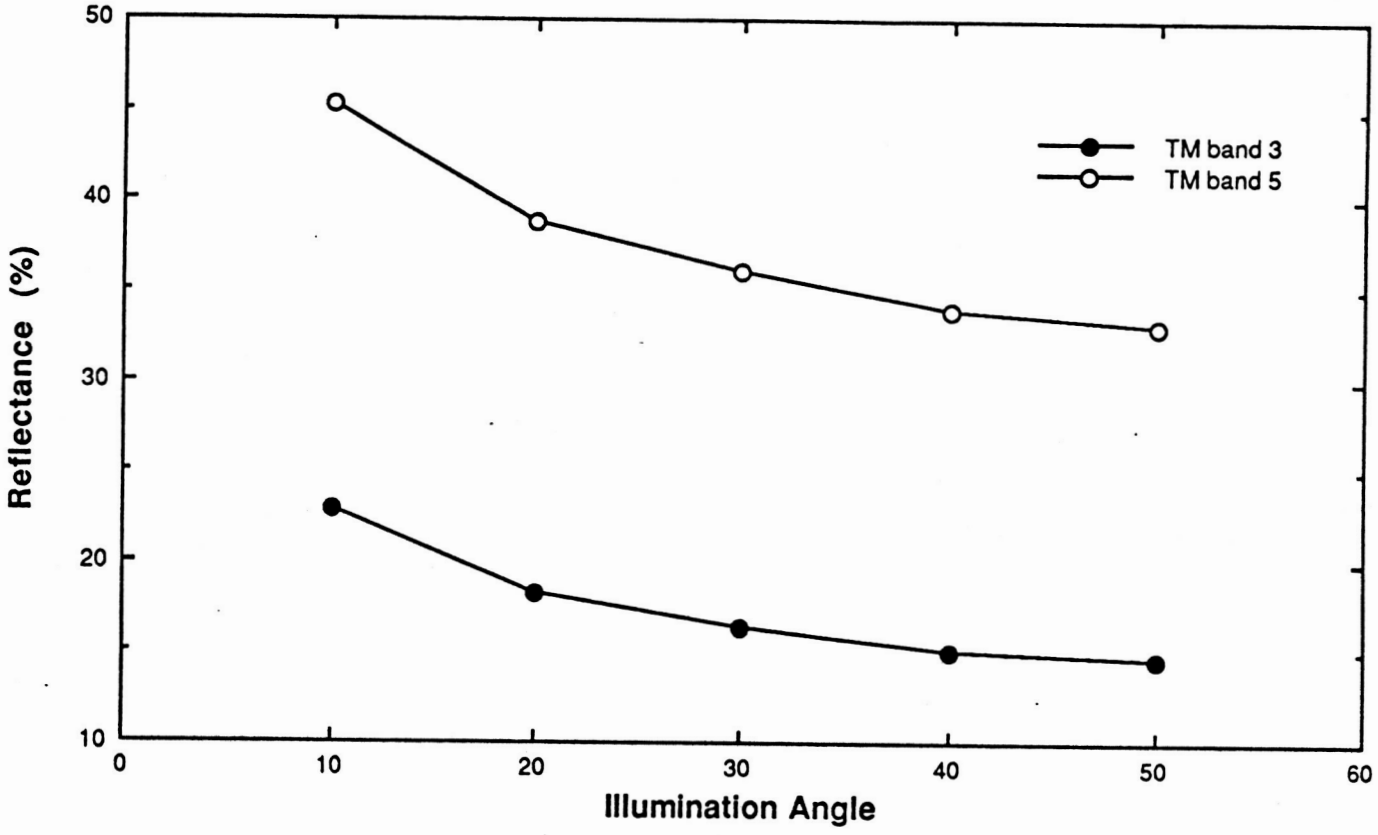
50
40
30
20
10
0
10
20
30
40
50
60
Reflectance (%)
Illumination Angle
TM band 3
TM band 5

Figure 6.

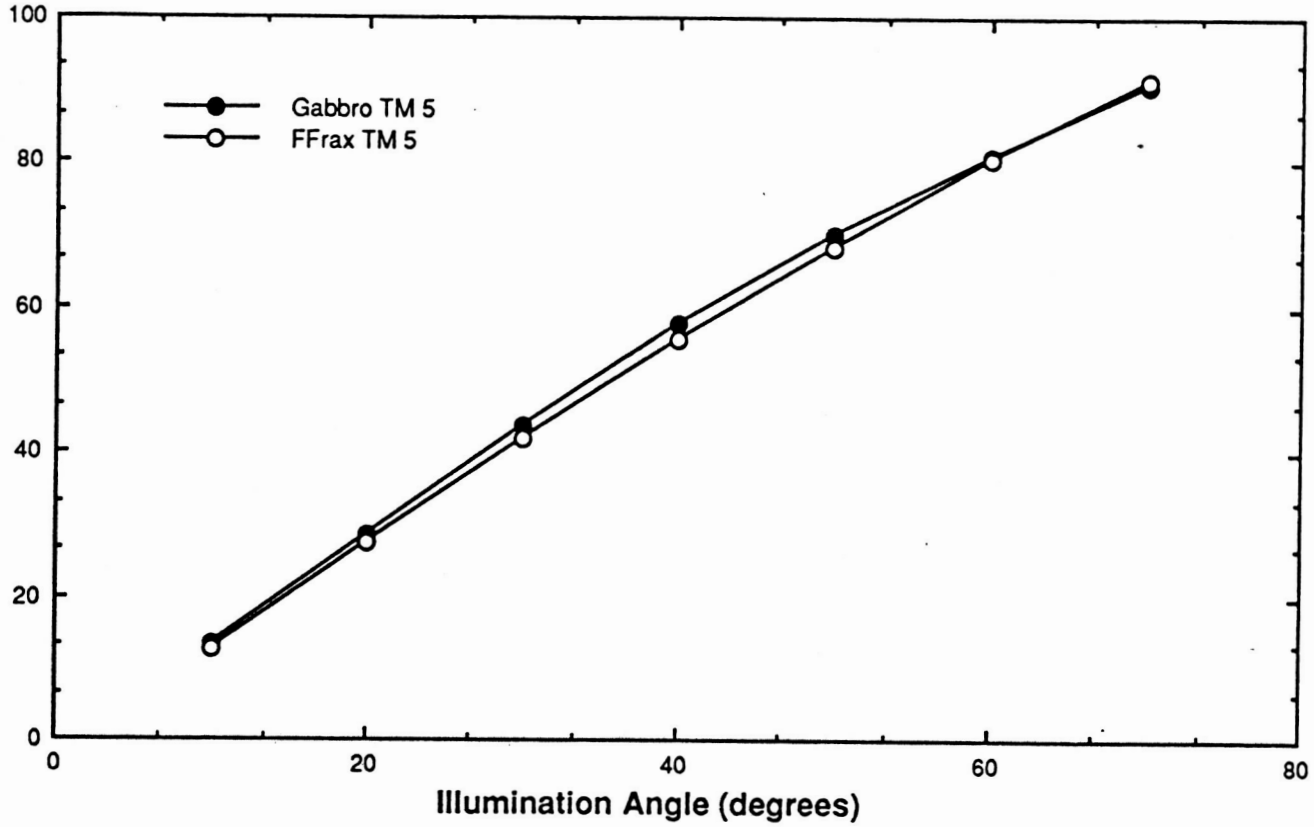

Figure 7.

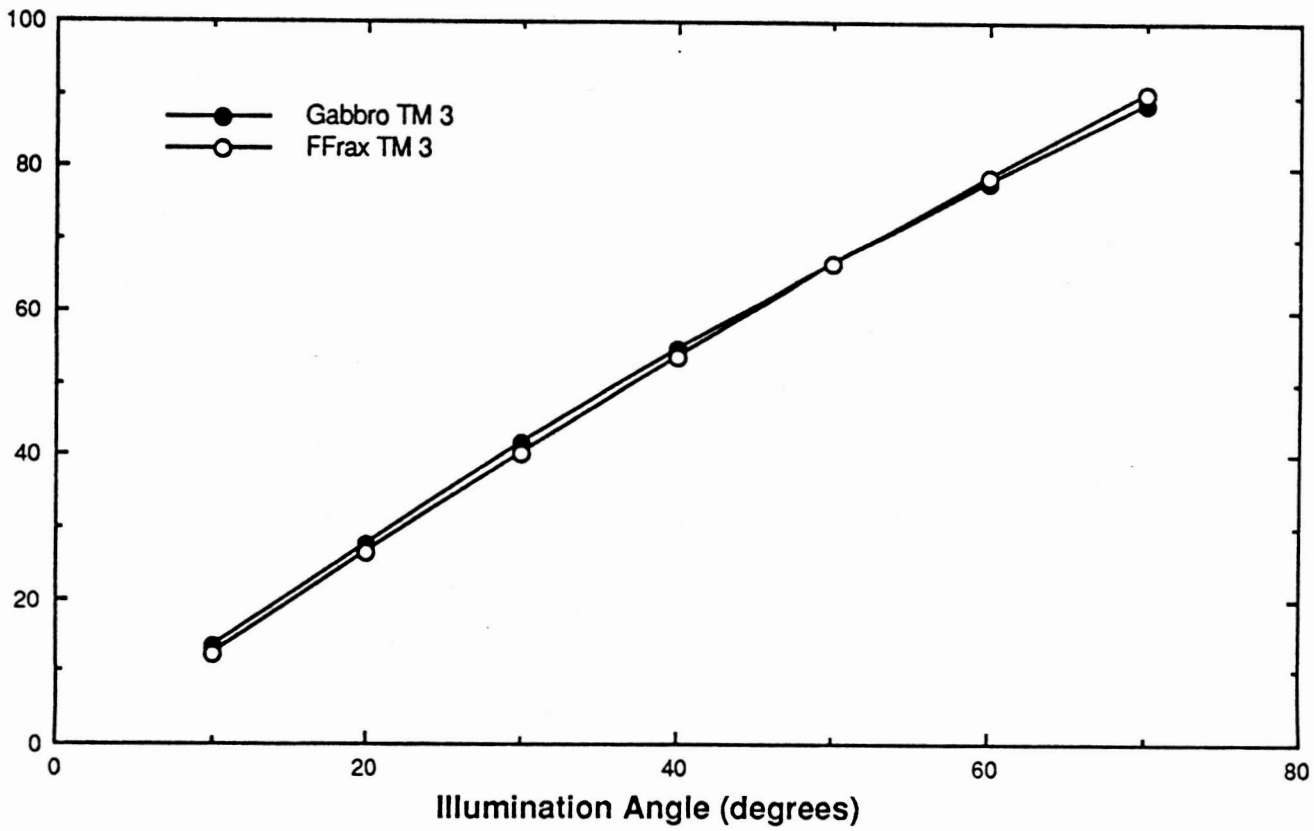

Figure 8.

Appendix 3

TM Imagery of the Skaergaard intrusive center.

Image 1 - Bands 2, 3, and 4 false color image (504 x 504 pixels).

Image 2 - Bands 3, 4, and 5 false color image (504 x 504 pixels).

Image 3 - Band ratio 5/1 image with blue>green>yellow>red denoting increasing values (504 x 504 pixels).

Image 4 - Band ratio 5/3 image with blue>green>yellow>red denoting increasing values (504 x 504 pixels).

Image 5 - Band ratio 4/3 image with blue>green>yellow>red denoting increasing values (504 x 504 pixels).

Image 6 - Bands-Band Ratio 1, 3/1, and 5 false color image (504 x 504 pixels).

Image 7 - Band Ratios 4/3, 5/1, and 5/3 false color image (504 x 504 pixels).

Image 8 - Band Ratios 3/1, 4/3, and 5/3 false color image (504 x 504 pixels).

Image 9 - Band Ratios 3/1, 4/3, and 5/3 transformed and enhanced image (504 x 504 pixels).

Image 10 - 1st, 2nd, and 4th principal components false color image (504 x 504 pixels).

Image 11 - Supervised maximum likelihood classification image based on selected test sites (504 x 504 pixels).

Image 12 - Supervised maximum likelihood classification image based on selected test sites (504 x 504 pixels).

Image 1 - Bands 2, 3, and 4 false color image (504 x 504 pixels).

Image 2 - Bands 3, 4, and 5 false color image (504 x 504 pixels).

Image 3 - Band ratio 5/1 image with blue>green>yellow>red denoting increasing values (504 x 504 pixels).

Image 4 - Band ratio 5/3 image with blue>green>yellow>red denoting increasing values (504 x 504 pixels).

Image 5 - Band ratio 4/3 image with blue>green>yellow>red denoting increasing values (504 x 504 pixels).

Image 6 - Bands-Band Ratio 1, 3/1, and 5 false color image (504 x 504 pixels).

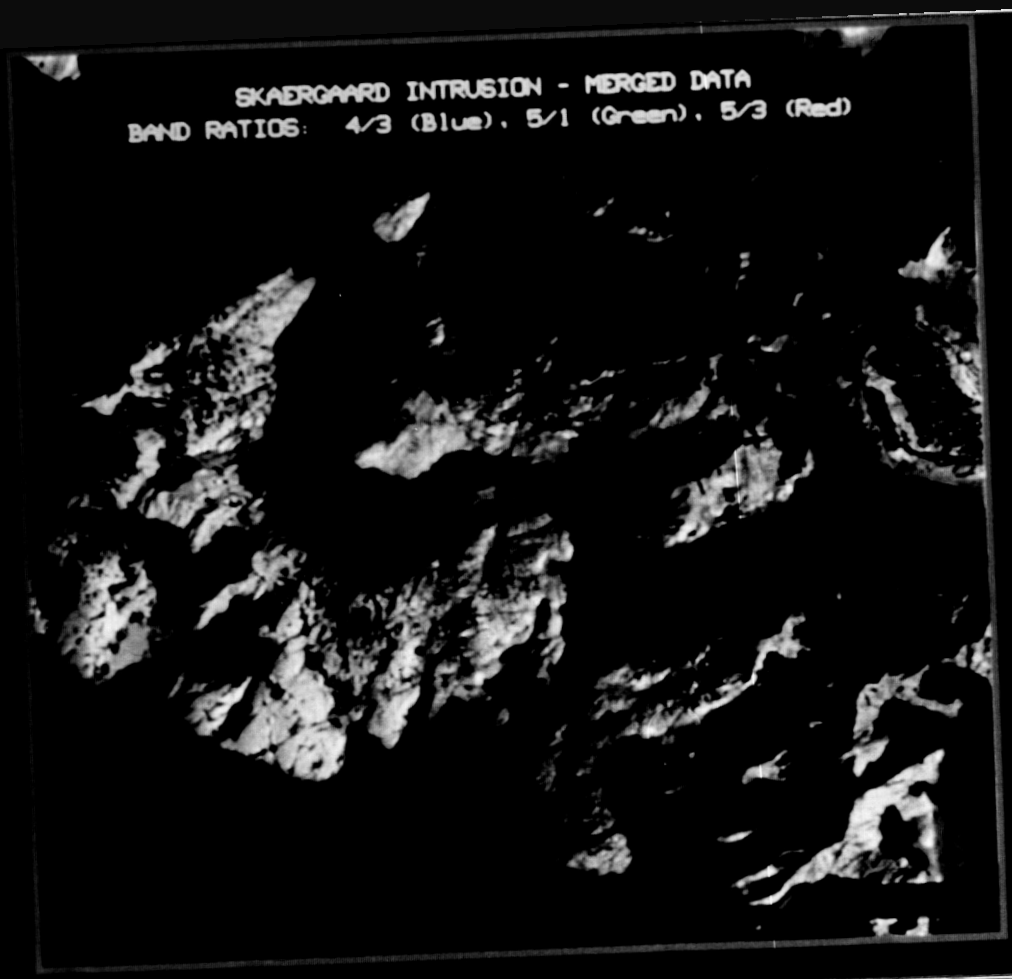

Image 7 - Band Ratios 4/3, 5/1, and 5/3 false color image (504 x 504 pixels).

Image 8 - Band Ratios 3/1, 4/3, and 5/3 false color image (504 x 504 pixels).

Image 9 - Band Ratios 3/1, 4/3, and 5/3 transformed and enhanced image (504 x 504 pixels).

Image 10 - 1st, 2nd, and 4th principal components false color image (504 x 504 pixels).

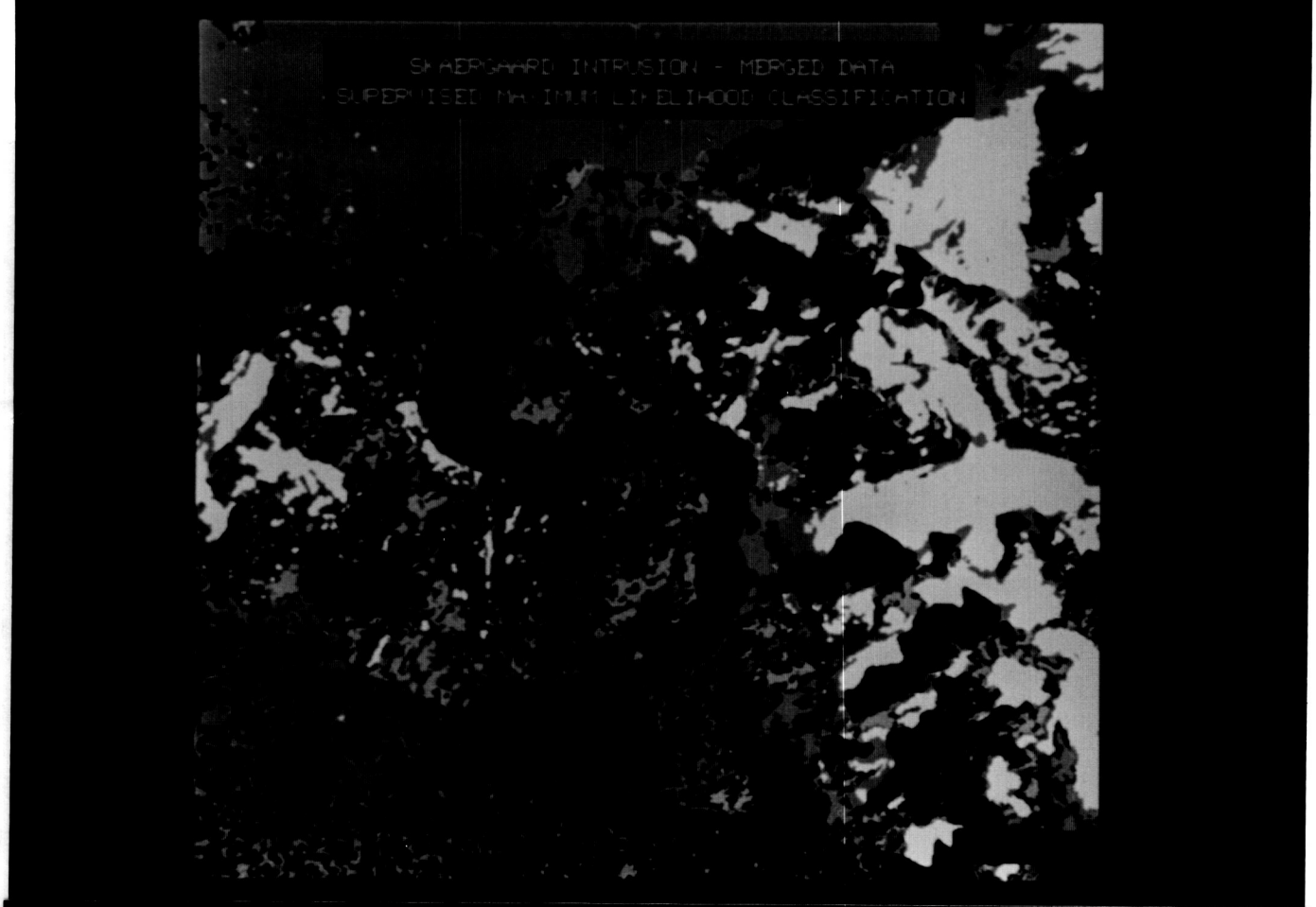

Image 11 - Supervised maximum likelihood classification image based on selected test sites (504 x 504 pixels).

Image 12 - Supervised maximum likelihood classification image based on selected test sites (504 x 504 pixels).

Appendix 4

TM Imagery of the Kangerdlugssuaq, Kap Edvard Holm, Gardiner, Kruuse Fjord, Imilik, Borgetinderne, and Lilloise intrusive centers

Image 13 - Bands 3, 4, and 5 false color image of the Kap Edvard Holm intrusive complex (1008 x 1008 pixels).

Image 14 - Bands 3, 4, and 5 false color image of the Kangerdlugssuaq intrusive complex (1008 x 1008 pixels).

Image 15 - Bands 3, 4, and 5 false color image of the southern half of the Kap Edvard Holm intrusive complex (504 x 504 pixels).

Image 16 - Bands 3, 4, and 5 false color image of the northern half of the Kap Edvard Holm intrusive complex (504 x 504 pixels).

Image 17 - Bands 3, 4, and 5 false color image of the north central part of the Kangerdlugssuaq intrusive complex (504 x 504 pixels).

Image 18 - Bands 3, 4, and 5 false color image of the northeastern part of the Kangerdlugssuaq intrusive complex (504 x 504 pixels).

Image 19 - Bands 3, 4, and 5 false color image of the Borgtinderne and Lilloise intrusions (2016 x 1344 pixels).

Image 20 - Bands 3, 4, and 5 false color image of the Lilloise intrusion (672 x 672 pixels).

Image 21 - Bands 3, 4, and 5 false color image of the Kruuse Fjord intrusive complex (1008 x 1008 pixels).

Image 22 - Bands 3, 4, and 5 false color image of the Imilik intrusive complex (1512 x 1512 pixels).

Image 23 - Bands 3, 4, and 5 false color image of the Gardiner intrusive complex (504 x 504 pixels).

Image 13 - Bands 3, 4, and 5 false color image of the Kap Edvard Holm intrusive complex (1008 x 1008 pixels).

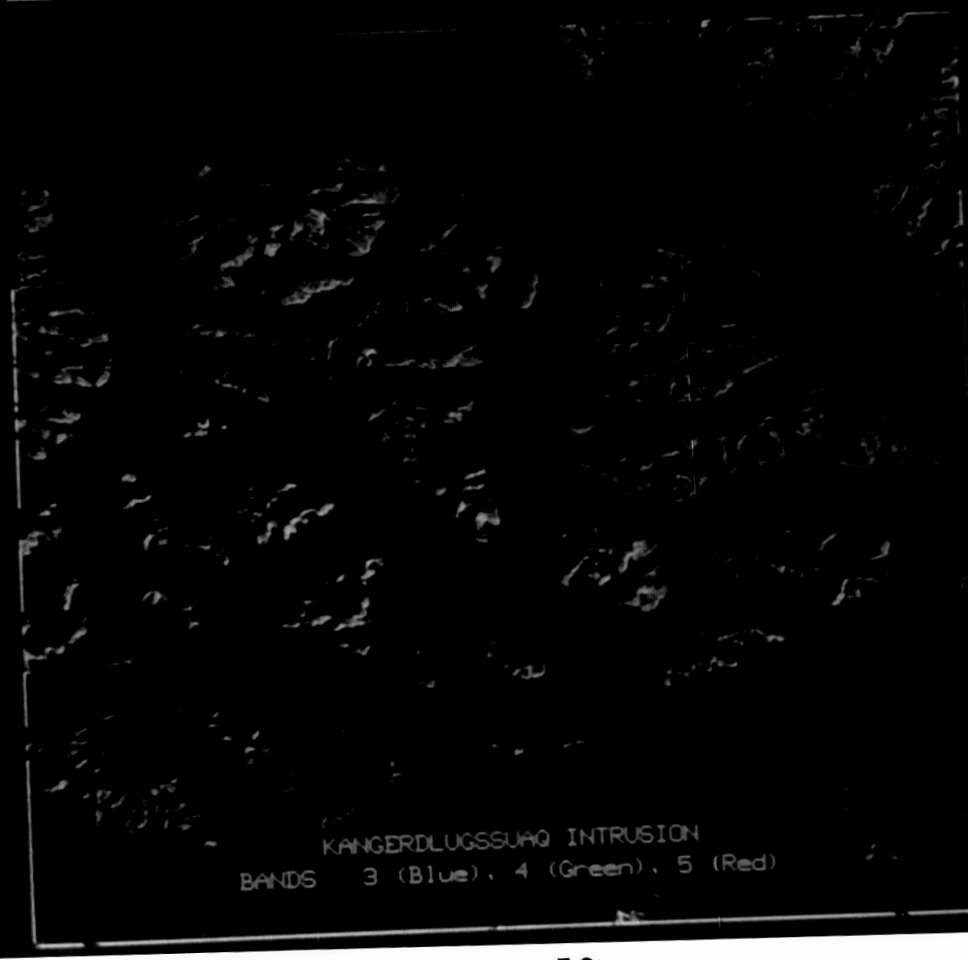

Image 14 - Bands 3, 4, and 5 false color image of the Kangerdlugssuaq intrusive complex (1008 x 1008 pixels).

Image 15 - Bands 3, 4, and 5 false color image of the southern half of the Kap Edvard Holm intrusive complex (504 x 504 pixels).

Image 16 - Bands 3, 4, and 5 false color image of the northern half of the Kap Edvard Holm intrusive complex (504 x 504 pixels).

Image 17 - Bands 3, 4, and 5 false color image of the north central part of the Kangerdlugssuaq intrusive complex (504 x 504 pixels).

Image 18 - Bands 3, 4, and 5 false color image of the northeastern part of the Kangerdlugssuaq intrusive complex (504 x 504 pixels).

Image 19 - Bands 3, 4, and 5 false color image of the Borglinderne and Lilloise intrusions (2016 x 1344 pixels).

Image 20 - Bands 3, 4, and 5 false color image of the Lilloise intrusion (672 x 672 pixels).

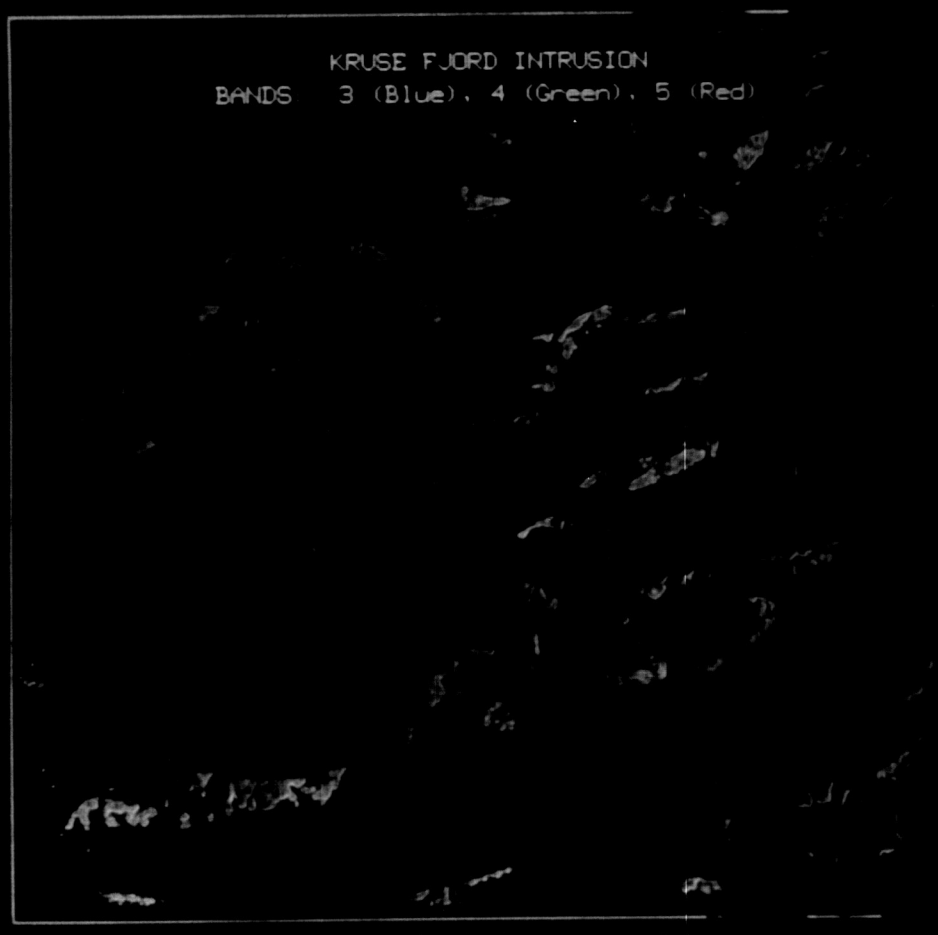

Image 21 - Bands 3, 4, and 5 false color image of the Kruuse Fjord intrusive complex (1008 x 1008 pixels).

Image 22 - Bands 3, 4, and 5 false color image of the Imilik intrusive complex (1512 x 1512 pixels).

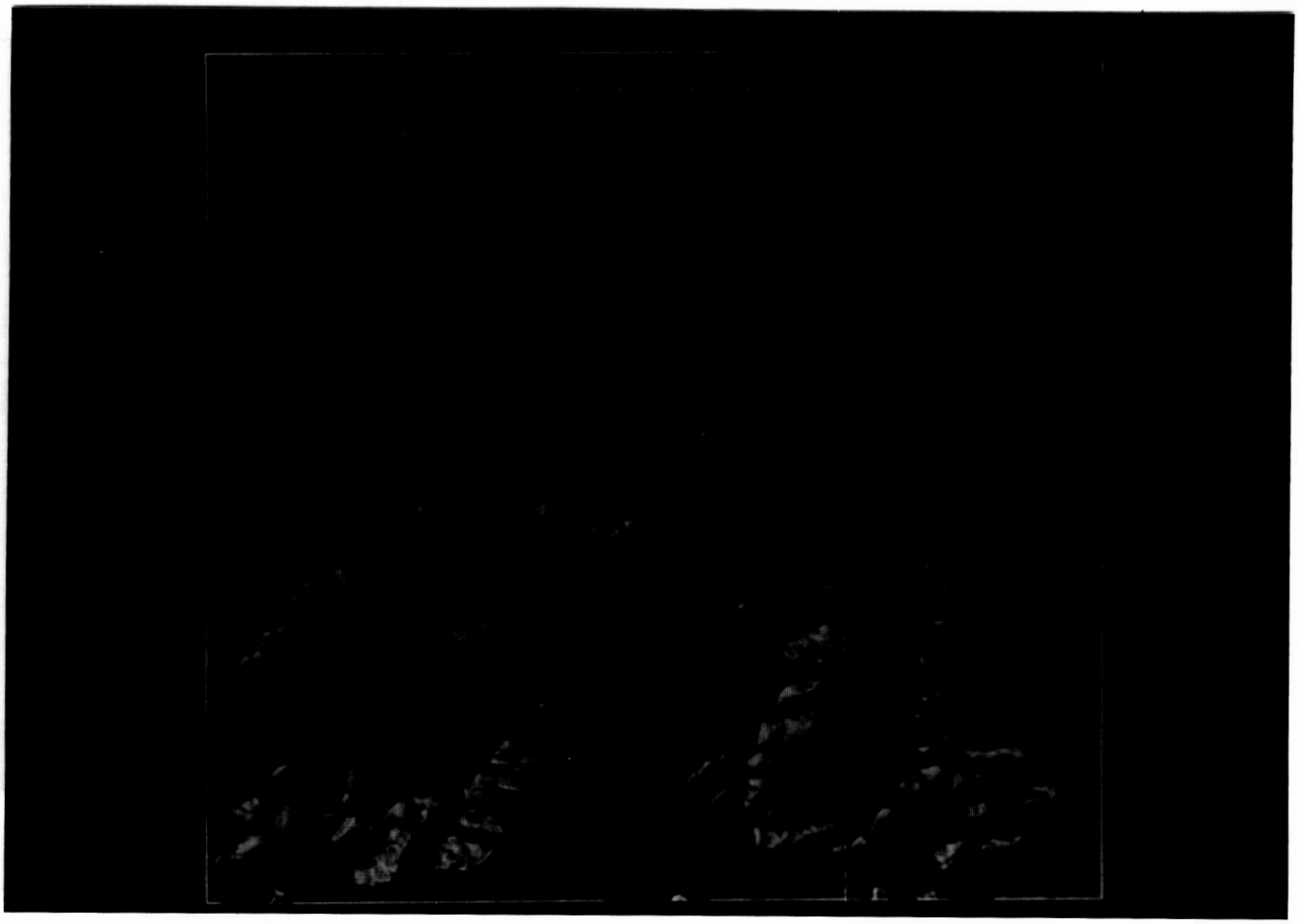

Image 23 - Bands 3, 4, and 5 false color image of the Gardiner intrusive complex (504 x 504 pixels).